

Natural Frequency Based Damage Identification of Beams
Using Piezoelectric Materials

by

Shengjie Zhao

A thesis submitted to the Faculty of Graduate Studies of the University of Manitoba
in partial fulfilment of the requirements of the degree of

MASTER OF SCIENCE

Department of Mechanical Engineering
University of Manitoba
Winnipeg

Copyright © 2016 by Shengjie Zhao

Abstract

Following the studies of natural frequency based damage detection methods, an advanced technique for damage detection and localization in beam-type structures using a vibration characteristic tuning procedure is developed by an optimal design of piezoelectric materials. Piezoelectric sensors and actuators are mounted on the surface of the host beam to generate excitations for the tuning via a feedback process. The excitations induced by the piezoelectric effect are used to magnify the effect of the damage on the change of the natural frequencies of the damaged structure to realize the high detection sensitivity. Based on the vibration characteristic tuning procedure, a scan-tuning methodology for damage detection and localization is proposed. From analytical simulations, both crack and delamination damage in the beams are detected and located with over 20% change in the natural frequencies. Finite element method (FEM) simulations are conducted to verify the effectiveness of the proposed methodology.

Acknowledgements

I would like to take this opportunity to thank my advisor, Dr. Nan Wu, for his constant support and great patience. The door of his office was always open to me whenever I got into trouble about my research or writing. It is an honor for me to work under his supervision.

I would also like to thank colleagues in our laboratory. My sincere thanks also goes to professors who provided me useful help during my Master study.

Finally, I would like to thank my family for the unconditional love and endless support.

Contents

Abstract.....	I
Acknowledgements.....	II
Contents	III
List of Tables	V
List of Figures.....	VI
List of Symbols.....	IX
1. Introduction.....	1
1.1 Background.....	1
1.2 Literature review.....	3
1.2.1 Classification of vibration based damage identification methods.....	3
1.2.2 Natural frequency based methods in damage identification.....	5
1.2.3 The use of piezoelectric materials in damage identification.....	7
1.3 Research objectives.....	11
2. Basic of theoretical models.....	13
2.1 Model of a vibrating beam.....	13
2.2 Model of piezoelectric effect.....	14
2.3 Model of a damage.....	17
3. Crack detection of beams by a vibration characteristics tuning technique through an optimal design of piezoelectric layers.....	18

3.1 Theoretical models.....	18
3.2 Simulations and discussions	25
3.3 Summary.....	27
4. Crack identification through a scan-tuning process using piezoelectric materials	37
4.1 Theoretical model	38
4.2 Numerical simulations and discussions	41
4.3 Finite element method simulations	45
4.4 Summary.....	46
5. Delamination identification through a scan-tuning process using piezoelectric materials...	63
5.1 Theoretical model	63
5.2 Simulations and discussions	64
5.3 Summary.....	67
6. Conclusions and future works.....	74
Reference	77
Appendix A Linear piezoelectric constitutive equations (LPCE).....	84
Appendix B Boundary and continuity conditions of beams under scan vibration tuning for crack identification	86
Appendix C Boundary and continuity conditions of beams under scan vibration tuning for delamination identification	89
Appendix D List of publications.....	96

List of Tables

Table 3-1 Geometric and material properties for numerical simulations	29
Table 3-2 Difference in natural frequencies for healthy and cracked beams in traditional method	30
Table 4-1 The definition of the L_a , L_b and L_c	48
Table 4-2 Geometric and material properties for numerical simulations	49
Table 4-3 Difference in natural frequencies for healthy and cracked beams ($L_c=0.32\text{m}$, $d=0.012\text{m}$)	50
Table 4-4 Difference in natural frequencies of healthy and cracked beams in FEM simulation without vibration tuning.....	50
Table 4-5 Difference in natural frequencies of healthy and cracked beams in FEM simulation with vibration tuning at appropriate position.....	51
Table 5-1 Geometric and material properties for numerical simulations	68
Table 5-2 Difference in natural frequencies for healthy and delaminated beams without vibration tuning ($L_{d1}=0.22\text{m}$, $L_{d2}=0.32\text{m}$)	69
Table 5-3 Difference in natural frequencies for healthy and delaminated beams without vibration tuning ($L_{d1}=0.10\text{m}$, $L_{d2}=0.15\text{m}$)	69

List of Figures

Fig. 1-1 Classification of vibration based damage identification approaches.	12
Fig. 3-1 Procedure of vibration characteristic tuning.	30
Fig. 3-2 Cantilevered beams with and without a crack at the fixed end.	31
Fig. 3-3 Cantilevered beams with and without a crack at the middle.	31
Fig. 3-4 Difference of the 1st natural frequency between the cracked and intact beams with vibration characteristic tuning versus gain factor for $d=0.004\text{m}$, $L_1=0.02\text{m}$ and $L_2 =0.81\text{m}$	32
Fig. 3-5 Variation in 1st nature frequency due to a crack ($d=0.004\text{m}$) versus location of the piezoelectric layer with certain length, $L_2-L_1=0.79\text{ m}$, and a fixed gain factor, $g=160$	33
Fig. 3-6 Change in 1st nature frequency due to a crack ($d=0.004\text{m}$) versus length of the piezoelectric layer located at a fixed location, $L_1=0.01\text{m}$, with a fixed gain factor, $g=160$	34
Fig. 3-7 Difference in the 1 st natural frequency between cracked and intact beams with vibration characteristic tuning versus gain factor for $d=0.002\text{m}$, $L_1=0.005\text{m}$ and $L_2 =0.5\text{m}$	35
Fig. 3-8 Changes in 1 st and 2 nd natural frequency due to a crack at the midspan for different gain factors.	36
Fig. 4-1 Procedure of scan vibration tuning method.	52
Fig. 4-2 Physical model of a cracked cantilever beam coupled with piezoelectric patches.	53
Fig. 4-3 The change in the natural frequencies of the cantilever beam due to the crack effect with different gain under the scan-tuning, where the values for $L_c=0.32\text{ m}$, $L_1=0.31\text{m}$, $d=0.0012\text{m}$...	53
Fig. 4-4 The change in the natural frequencies of the cantilever beam due to the crack effect under the scan-tuning, where the values for $L_c=0.32\text{ m}$, $d=0.0012\text{m}$ and $g=8.5$	54
Fig. 4-5 Mode shapes of the cantilever beam with the activation of the piezoelectric actuator with different locations, where the values for $L_c=0.32\text{ m}$, $d=0.0012\text{m}$ and $g=8.5$	55

Fig. 4-6 The non-dimensional curvature distribution of the healthy cantilever beam without tuning.	57
Fig. 4-7 The change in the natural frequencies of the cantilever beam due to the crack effect with different depth of the crack under the scan-tuning, where the values for $L_c=0.32$ m, $d=0.0012$, $g=8$	58
Fig. 4-8 The change in the natural frequencies of the cantilever beam due to the crack effect with different locations of the crack under the feedback excitation of the piezoelectric actuator that is close to the crack, where the values for $a=0.0012$ m and $g=8$	59
Fig. 4-9 The changes in the natural frequencies of the cantilever beam due to the crack with different depth under the scan-tuning with the fixed values of $L_c =0.32$ m, $L_I=0.31$ m, $g=8.5$	60
Fig. 4-10 Finite element model of a cantilever beam with a crack at $L_c=0.32$ m	61
Fig. 4-11 Frequency spectrums of FEM simulations (a) without vibration tuning and (b) with vibration tuning at appropriate position.....	62
Fig. 5-1 Physical model of a delaminated cantilever beam coupled with piezoelectric patches ..	70
Fig. 5-2 The change in the natural frequencies of the cantilever beam due to the delamination effect under the scan-tuning, where the values for $L_{d1}=0.22$ m, $L_{d2}=0.32$ m, $l_p=0.06$ m and $g=6$	70
Fig. 5-3 The change in the natural frequencies of the cantilever beam due to the delamination effect under the scan-tuning, where the values for for $L_{d1}=0.22$ m, $L_{d2}=0.32$ m, $l_p=0.03$ m and $g=6$	71
Fig. 5-4 The change in the natural frequencies of the cantilever beam due to the delamination effect under the scan-tuning, where the values for $L_{d1}=0.22$ m, $L_{d2}=0.32$ m, $l_p=0.01$ m and $g=6$	72
Fig. 5-5 The change in the natural frequencies of the cantilever beam due to the delamination effect under the scan-tuning, where the values for $L_{d1}=0.10$ m, $L_{d2}=0.15$ m, $l_p=0.01$ m and $g=6$	73

Fig. C-1 Physical model of a delaminated beam coupled with piezoelectric patches when $L_2 < L_{d1}$
..... 94

Fig. C-2 Physical model of a delaminated beam coupled with piezoelectric patches when $L_1 < L_{d1}$
and $L_2 > L_{d1}$ 94

Fig. C-3 Physical model of a delaminated beam coupled with piezoelectric patches when $L_1 > L_{d1}$
and $L_2 < L_{d2}$ 94

Fig. C-4 Physical model of a delaminated beam coupled with piezoelectric patches when $L_1 < L_{d2}$
and $L_2 > L_{d2}$ 95

Fig. C-5 Physical model of a delaminated beam coupled with piezoelectric patches when $L_1 > L_{d2}$
..... 95

List of Symbols

- E : Young's modulus of the host beam
- E_p : Young's modulus of piezoelectric materials
- ρ : Density of the host beam
- ρ_p : Density of piezoelectric materials
- m : Mass of the host beam
- m' : Mass of the piezoelectric coupled beam
- I : Moment of inertia of the host beam
- I_p : Moment of inertia of the piezoelectric layers
- L : Length of the host beam
- L_1 : Position of the left end of the piezoelectric patch/ layer
- L_2 : Position of the right end of the piezoelectric patch/ layer
- L_{d1} : Position of the left end of the delamination
- L_{d2} : Position of the left end of the delamination
- h : Height of the host beam
- h_1 : Thickness of the piezoelectric patch/ layer
- h_{d1} : Height of the upper delaminated beam section
- h_{d2} : Height of the lower delaminated beam section
- b : Width of the host beam
- b_s : Width of the piezoelectric sensor
- b_a : Width of the piezoelectric actuator
- l_p : Length of single piezoelectric patch
- d : Depth of the crack
- N : Number of beam sections

- n : Indication of n^{th} couple of piezoelectric patches
- w : Displacement of the host beam
- β : Natural frequency related constant
- ω : Natural frequencies of the beam
- Me : Bending moments induced by piezoelectric materials
- Q : Electrical charge on the surface of piezoelectric sensor
- V_s : Voltage output of the piezoelectric sensor
- V_a : Voltage input of the piezoelectric actuator
- g : Gain of the voltage amplifier
- S : Shear force induced by piezoelectric materials
- θ : Slope discontinuity
- e_{31} : Piezoelectric coupling coefficients for Stress-Charge form
- d_{31} : Piezoelectric coupling coefficients for Strain-Charge form
- C_v : Electrical capacity of the piezoelectric materials

1. Introduction

1.1 Background

Damages, such as cracks, delamination and corrosions, are usually inevitable in engineering structures during their daily operations especially in the overstressed areas. Severe accidents may be caused by stress concentration and propagation of the damages. Therefore, structure health monitoring (SHM), a developed discipline, has attracted considerable attention in recent decades. It is generally accepted that the broad range of techniques in SHM can be classified into four levels as follows [1]:

- Level 1: Determination that damage is present in the structure;
- Level 2: Determination of the geometric location of the damage;
- Level 3: Quantification of the severity of the damage;
- Level 4: Prediction of the remaining service life of the structure.

Focusing on the levels 1-3, vibration-based damage detection has been commonly used for structural health monitoring and was first applied in the late 1970s [2, 3]. Because of the simple measurement of the natural frequencies, natural frequency based methods have been thoroughly studied for a long while. With the change of the structural stiffness or mass when a damage occurs and propagates, the natural frequencies are supposed to be altered, which can be monitored by only one single sensor. However, the limitations and shortcomings [4] of the natural frequency based methods are obvious. The greatest problem for this type of methods is the low sensitivity on small damages. Besides, the uniqueness of the detection results remains to be proven. Thus, new techniques are necessary to further develop the natural frequency based methods rather than

making a direct comparison between the measured natural frequencies from the monitored structure and the healthy structure.

Recently, the smart materials are widely employed for SHM to provide richer data for analysis. Among those materials, piezoelectric materials are one of the commonest type of smart materials to realize the effective control on the smart structures. Piezoelectric materials are able to generate electrical charge under mechanical force, and vice versa. Owing such a unique characteristic, piezoelectric materials have been widely used as sensors and actuators in engineering structures [5-8]. Nevertheless, the use of piezoelectric materials for active control in damage identification is limited.

To apply the piezoelectric materials for the damage identification to monitored structures, the piezoelectric layers or patches are usually mounted on the surface or embedded in the host structures to realize the active control on the host structure [9]. The damage effect on the natural frequencies of the structure is expected to be magnified with decent control process. In this thesis, the mechanism of the active control process for beam damage detection coupled with piezoelectric materials is proposed. The optimal size and placement of the piezoelectric materials are also discussed. In addition, inspired by the proposed mechanism, a scan vibration tuning methodology for damage identification is studied on cracked beams and delaminated beams. A finite element model is provided to verify this methodology as well.

1.2 Literature review

In this section, the literature review of previous studies is conducted. The classification of the vibration based damage identification methods is firstly listed. Focusing on the natural frequency based method, the pros and cons of the previous research are discussed, followed by the review of the applications of piezoelectric materials in damage identification.

1.2.1 Classification of vibration based damage identification methods

In the past decades, various vibration testing techniques have been developed for damage identification. According to Carden and Fanning's review[2], the previous damage identification approaches based on the vibration characteristics can be categorized as Fig. 1-1. There is no absolutely optimal method using vibration data for damage detection. The selection of the detection methods usually depends on the type of damage and the type of the monitored structure. A brief review on current mainstream methods with typical research outcomes are summarized.

- Natural Frequency Based Methods

Damages induce a decrease in structural stiffness or mass, leading to reduction of the structural natural frequencies. With simple measurement, the damage may be detected by the frequency shift. Its potential in damage localization and quantification is also found [10, 11]. The detailed review of natural frequency based methods is shown in the following section.

- Mode Shape Based Methods

The damages may be identified by the comparison on measured mode shapes or mode shape curvatures [12-15]. Many modal analysis techniques are available for the mode shapes extraction from time-domain signals [16, 17]. However, the uncertainty of the mode shape based methods is

also doubted by many researchers due to the complicated formulations and the requirement of measured data from various locations of the structure. Such uncertainty also exists in other methods that use complex formulations, such as operational deflection shape based methods and modal energy based methods[2].

- Operational deflection shape based methods

Operational Deflection Shapes (ODS) analysis provide visualization of the vibration patterns (e.g. displacement and velocity) of the structure under a specific structural loading[18]. With the FEM simulations and experimental study, Waldron [19] successfully detected a 10% crack of a fixed-fixed beam under excitations from piezoelectric actuators by using a scanning laser Doppler vibrometer. The high sensitivity of ODS based damage detection methods is also verified by later research[20, 21].

- Modal Strain Energy based methods

Modal strain energy is also considered as a damage-sensitive feature to identify the structural damages. The modal strain energy in beam-type or plate-type structures, can be calculated from mode shape curvature[2, 22]. The previous works generally focused on 1-D strain methods [23-25]. The universality of the methods utilizing modal strain energy remains to be doubted.

- Statistical Methods

In Farrar and Doebling's opinion [26], vibration based damage detection problem is basically one of the statistic pattern recognition. To improve the state of the art of vibration based damage detection, the non-model based pattern recognition methods are in demand. Although this type of methods can efficiently detect the structural damages by only the statistical techniques without

building a complex numerical model [27-30], it lack the ability of damage localization and quantification.

1.2.2 Natural frequency based methods in damage identification

As a highly feasible technique, natural frequency based methods have been well studied for the past few years. Dating back to 1970s', the change of natural frequencies was initially studied to determine the damage in structures. Adams and Cawley [31] found the damage effect on the natural frequencies of longitudinal vibration. In 1990s', numerous researchers [32, 33] attempted to utilize the natural frequencies to detect the damage in multiple types of structures. The damage was determined by comparing the natural frequencies of the damaged structure with the healthy one. The location and severity of the damage were also studied through processing the frequency data. However, the detection sensitivity of the early studies is relatively low (less than 3% of natural frequency shift). For the practical measurement, at least 5% change in frequency is required for damage detection with confidence[34]. The uncertainty of the uniqueness of the detection result from natural frequency change is also doubted by Salawu[4].

In recent years, Zhong et al. [35] proposed a new approach based on auxiliary mass spatial probing using spectral centre correction method (SCCM) for damage detection. Accurate natural frequency, amplitude and phase were provided by SCCM to detect the crack damage in beam-type structures. The noise was also considered in vibration response from numerical simulations. However, the proposed approach is based on FEM simulation without theoretical explanation. It is not reasonable to verify the effectiveness of the approach by studying only one case of the crack location.

Wang [36] introduced a study on natural-frequency-based structural damage identification of steel transmission tower. A typical 110 kV self-supporting steel transmission tower was studied based on the 3D finite element model. However, a single damage in the structure induce fairly slight change in the low orders of natural frequencies for damage detection. The expansion of the case study to other types of structures was not discussed either.

Wang and Li [37] also developed a new method, iterative modal strain energy (IMSE) method, for damage localization and severity estimation requiring only the lower natural frequencies. Multi-damage scenarios in free beam structure and a plane frame structure were investigated by the FEM simulations. The experimental study further verified the effectiveness of the proposed method. However, the noise interruption during the measurement has not been discussed. The reliability of the proposed method in practical cases under environmental noise was not proven.

In 2014, Chao et al. [38] published a systematic method for damage assessment, including damage localization and damage quantification using output-only measurement. The practicability was verified by a finite element model and an experiment on a 6-story steel frame structure with different depths of member cut. Although the simulation results correctly assess the structural damage, the complexed algorithm derived from the natural frequencies increased the uncertainty of the method, while the measurement sensitivity of the modal frequencies was not enhanced either.

Negru1 et al. [39] presented their research on Natural frequency changes due to damage in composite beams. From numerical simulations, a unique curve representing the frequency change of transverse modes in respect to damage depth exists was shown. But again, the frequency change due to the damage did not reach the requirement for practical measurement.

In summary, the presence of the structural damage must change the natural frequencies of the structure to some extent. The simple measurement and limited number of sensors requirement make natural frequency based methods highly feasible. Nevertheless, the shortcomings of the traditional natural frequency based methods without active control are observable. The biggest problem is that the structural damage effect on the change of natural frequencies is usually tiny, while measurement of frequencies is extremely sensitive to the environmental noise. In this case, small damage might be ignored while only observing the natural frequencies. Another limitation is that identified damage from the change of natural frequencies is not definitely unique, which may cause the detection results ill-posed [4, 22]. Hence the damage location cannot be accurately and correctly recognized merely by the natural frequency changes.

1.2.3 The use of piezoelectric materials in damage identification

Smart materials have been widely use in smart structures for various purposes in SHM. Commonly used smart materials include piezoelectric materials, electro-rheological fluids, shape-memory materials, magnetostrictive materials, electrostrictive materials and thermal materials [40]. Because of the low cost, easy installation and unique piezoelectric effect, piezoelectric materials have become the top choice in numerous applications, for instance, structural damage repair [6, 7, 41, 42]. Nevertheless, the previous applications of piezoelectric materials in damage detection are mostly performed by finite element models or experiments, while the explanations of the theory are inadequate. The expansion of the use of piezoelectric materials in damage detection is hence restricted.

According to the reviewed literatures, the applications of piezoelectric materials in damage identification were relatively limited. Even for the piezoelectric materials used in the damage identification, mostly they are individually functioned as sensors or actuators. As early researchers

who utilized piezoelectric materials in this field, Islam and Craig [43] described a method for damage detection in composite structures by embedded piezoelectric sensors and actuators. The backpropagation neural network models were developed to predict the delamination size and location. Although this method revealed a huge potential from the piezoelectric materials in damage detection, still, the variation in natural frequencies due to the damage is too tiny for measurement in real applications. The neural network also produced uncertainty of the proposed method. Investigations based on the similar idea were also done by other researchers [44-47] to show the possibility to build up a damage identification system with the piezoelectric materials, but the common issues like the uniqueness of the results and the interference of the noise have not been solved.

De Vera et al. [48] suggested a frequency-based method based on self-sensing piezoelectric on damage detection. The bridge electronic circuit for self-sensing and the control process were illustrated. By exciting the structure at different frequencies and analyzing its response, the feature of the damage in the structure was detected. The damage was obtained by machining a hole with different sizes. The temperature changes influence was also studied to more accurately determine the damage. However, the damage effect was insignificant in low order natural frequencies, and the theoretical dynamic model has not been established. The localization of the damage could not be determined by the proposed method either.

In 2002, Su et al.[49] proposed an identification approach for delamination locating in laminated composites based on wave propagation. Distributed piezoelectric transducers were employed to generate and monitor the ultrasonic Lamb wave with narrowband frequency. The diagnostic system was explained in details and verified by quasi-isotropic CF/EP composite laminates, but further discussion of the delamination evaluation was required. Liu et al. [50] further investigated

the design of PZT actuator/sensor, which were employed to generate the lamb wave for damage detection.

More recently, in 2006, Hadjigeorgiou et al. [51] reported their research about shape control and damage identification. Piezoelectric patches were employed as actuators to provide the control forces. The damage identification problem was solved by the static data from beam deformation on finite element models. Optimal design of the piezoelectric actuators was conducted through the genetic optimization. The damage identification results were significant based on the numerical simulations. However, the precise measurement of the deformation of the beam requires numerous vibration sensors or laser vibrometer. Hence, the cost of the proposed method would be much higher than the natural frequency based method. Besides, the accuracy of the deflection measurement is also hard to be guaranteed, which may lead to incorrect damage prediction.

Jiang et al. [52, 53] proposed another scheme that utilizes the piezoelectric transducer circuitry with tunable inductance to enrich the frequency-shift data. By tuning the inductance, the variation of the vibration response can be characterized more completely and accurately. An iterative second-order perturbation-based algorithm in conjunction with an optimization scheme was also developed to figure out the frequency shift due to the structural damage occurrence. Following this scheme, Zhao et al. [54] brought an improvement of the proposed methodology with a statistical damage identification algorithm which was formulated to minimize the uncertainty and noise effect. Based on the FEM simulations, the damage-induced frequency shift was enhanced by piezoelectric transducer circuitry. However, lacking of theoretical model, the practicality of the mentioned methods remains to be investigated.

Yang et al. [55] presented an experimental study of damage localization on an aluminum plate specimen. An array of nine PZT impedance transducers were subjected to electric actuation so as

to generate the electromechanical admittance. The damage location was located from the root mean square deviation value. Further study was needed to conduct the optimal design of the PZT placement and apply on other types of structures.

Bhalla et al. [56] proposed an advanced technique, the dynamic strain approach, for damage diagnosis of tensegrity structures by means of the piezoelectric materials. The damage was localized using changes in natural frequencies observed from experimental observations. It was proved that the dynamic strain approach is very expedient and sensitive for tensegrity structures. The damage locations were determined on the element number instead of the exact position. Further study of the proposed technique is required for damage detection in other structures.

Providakis et al. [57] tentatively detected the damages in the reinforcement bars of reinforced concrete members using piezoelectric materials. An integration approach based on both electromechanical admittance methodology and guided wave propagation technique was employed to identify the damages, which were reflected by the diameter reduction. The comparative results of the evaluated FFT admittance of the piezoelectric sensor between the healthy condition of the steel bar and the examined damaged states were very promising. The potential of the proposed technique in other types of structures or materials was not discussed yet.

Overall, the damage identification sensitivity was obviously enhanced by means of piezoelectric materials, but there has been no detailed theoretical model proposed to clearly describe the mechanisms of the damage detection sensitivity enhancement on continuous beam structures from the mechanical point of view. Therefore, the feasibility and efficiency are still pending to be verified. Meanwhile, the piezoelectric materials in the previous studies were individually performed as sensors or actuators, without producing feedback excitations. The unique piezoelectric effect has not been fully utilized in applications of damage identification.

1.3 Research objectives

From the literature review, the natural frequency based methods for damage identification were readily accessible, but insensitive to general damages. With the use of piezoelectric materials, the damage effect on the natural frequencies shift was enhanced to some extent. However, piezoelectric materials in most of the applications acted as only an individual sensor or actuator without any feedback control. Besides, most of the studies about damage identification coupled with piezoelectric materials are based on FEM simulations and experiments that cannot clearly explain the mechanism of the detection process.

In this thesis, a natural frequency based crack detection technique coupled with the piezoelectric materials on beam-type structures is proposed. Piezoelectric layers are applied on the surface of the host beams to generate the feedback control so as to magnify the crack effect on the natural frequencies. A theoretical model is provided to reveal the principle of the proposed technique with the feedback control process. Following this idea, a scan vibration tuning methodology by using multiple piezoelectric patches is proposed to detect and locate the damages in beam-type structures. Both the crack and delamination are effectively identified by the proposed methodology.

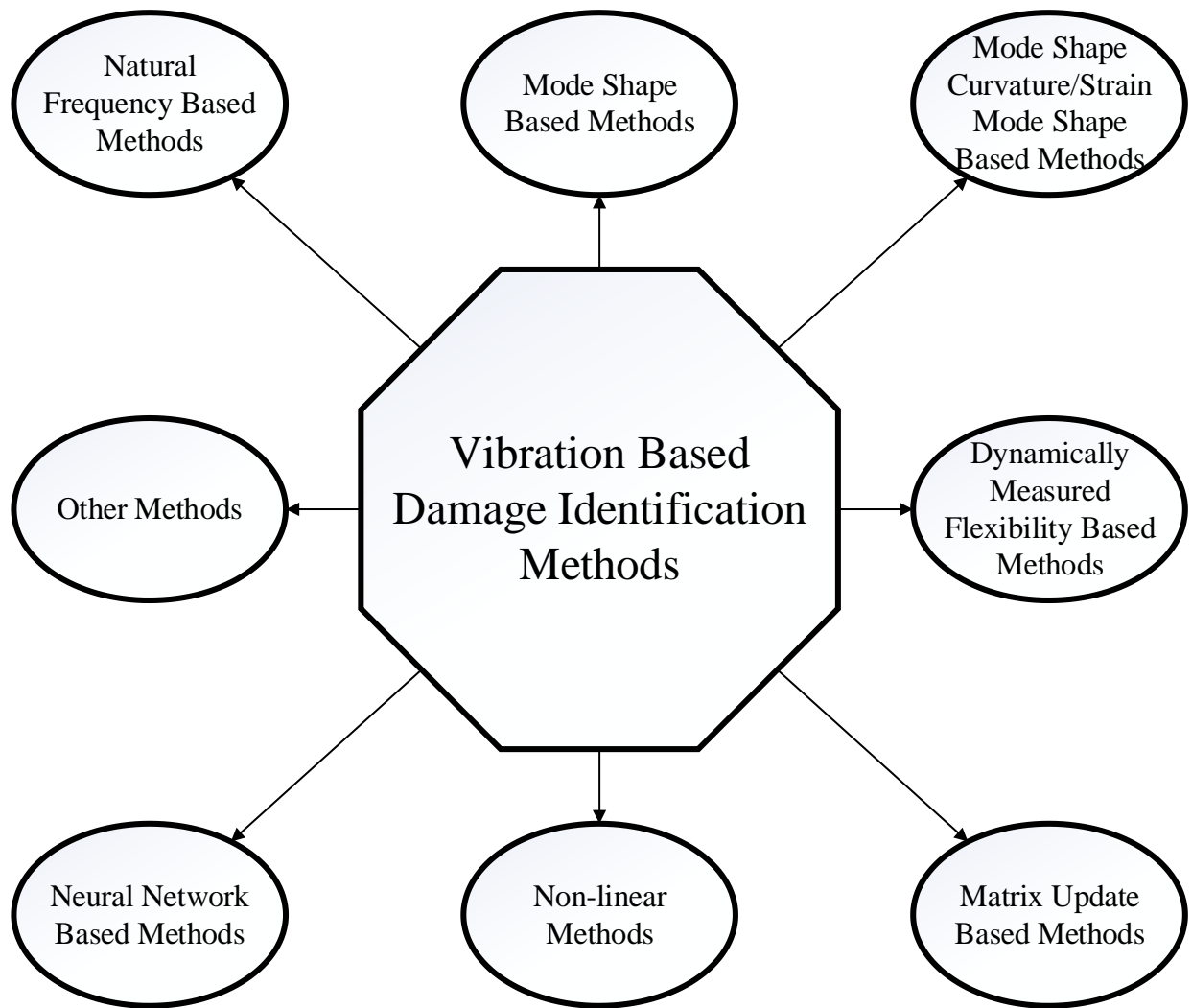


Fig. 1-1 Classification of vibration based damage identification approaches.

2. Basic of theoretical models

In this chapter, the basic of theoretical models of the damaged beams coupled with piezoelectric layers/ patches are provided. The continuous models of a vibrating beam is proposed first. Then the piezoelectric effect and damage effect on the beam model are explained. Both crack and delamination are taken into consideration as structural damages. Based on the provided formulations, the methodologies for damage detection and identification are presented with detailed theoretical models in the following chapters.

2.1 Model of a vibrating beam

Based on Euler-Bernoulli theory, the dynamic equation of a free-vibration beam can be written as

$$EI \frac{\partial^4 w_1(x,t)}{\partial x^4} + \rho b h \frac{\partial^2 w_1(x,t)}{\partial t^2} = 0, \quad (2-1)$$

where E is the Young's modulus of the host beam; ρ is the density of the host; b is the width of the host beam; h is the thickness of the host beam; I is the moment of inertia of the host beam given by $I = \frac{bh^3}{12}$; and $w(x, t)$ is the displacement of the beam in the transverse direction, which can be

expressed as follows for a certain vibration mode,

$$w(x,t) = W(x)T(t), \quad (2-2)$$

where $W(x)$ is the vibration mode shape function, and $T(t)$ is the time function.

The vibration mode shape function can be usually solved as

$$W(x) = C_1 \cos \beta x + C_2 \sin \beta x + C_3 \cosh \beta x + C_4 \sinh \beta x, \quad (2-3)$$

where C_{1-4} are natural constants, β is real constants related with the natural frequency of the beam given by

$$\beta = \sqrt[4]{\omega^2 \frac{\rho b h}{EI}}, \quad (2-4)$$

where ω is the natural frequency of the beam.

Substituting the vibration mode shape function and the expression of the piezoelectricity induced bending moments into the according boundary conditions and continuity conditions of the beam leads to a couple of linear equations. The vibration characteristics of the beam, including the natural frequencies, are solved from the eigenvalue problem on Matlab. The detailed vibration solutions of the damaged beam coupled with piezoelectric materials are illustrated in theoretical models of the later chapters.

2.2 Model of piezoelectric effect

To figure out the dynamic response of the piezoelectric coupled beams, the effect of the piezoelectric sensor and actuator is supposed to be determined first. The piezoelectric layers or patches are affixed on the surface of the thin cantilever beams to generate feedback vibration characteristic tuning excitations. The linear piezoelectric constitutive equations are listed in Appendix A. The simplified expression of the electrical charge generated on the surface of the piezoelectric sensor due to the bending of the host beam is given as [7, 58]

when piezoelectric layers/ patches are applied on the lower surface of the host beam:

$$Q = -e_{31} \int_{L_1}^{L_2} b_s \left(\frac{h}{2} + h_1 \right) \frac{d^2 w}{dx^2} dx, \quad (2-5)$$

when piezoelectric layers/ patches are applied on both surfaces of the host beam:

$$Q = -e_{31} \int_{L_1}^{L_2} b_s \left(\frac{h + h_1}{2} \right) \frac{d^2 w}{dx^2} dx, \quad (2-6)$$

where e_{31} is piezoelectric constant, b_s is the width of the piezoelectric sensor patch, L_1 and L_2 are the distances from the fixed end of the beam to the left and right ends of the piezoelectric layers respectively. Thus the output voltage of the piezoelectric sensor can be written as [7, 59]

when piezoelectric layers/ patches are applied on the lower surface of the host beam:

$$V_s = \frac{Q}{C_v} = -\frac{e_{31}b_s\left(\frac{h}{2} + h_1\right)}{C_v'} \int_{L_1}^{L_2} \frac{d^2w}{dx^2} dx, \quad (2-7)$$

when piezoelectric layers/ patches are applied on both surfaces of the host beam:

$$V_s = \frac{Q}{C_v} = -\frac{e_{31}b_s(h + h_1)}{2C_v'} \int_{L_1}^{L_2} \frac{d^2w}{dx^2} dx, \quad (2-8)$$

where C_v is the electrical capacity of the piezoelectric sensors, and $C_v' = \frac{C_v}{b_s}$ is electrical capacity per unit width of the piezoelectric sensors.

The voltage gathered from piezoelectric sensor is subsequently amplified with a designated feedback gain, g , which is a key factor in the tuning process. The piezoelectric actuator is then imposed by the amplified voltage given by

when piezoelectric layers/ patches are applied on the lower surface of the host beam:

$$V_a = gV_0 = -g \frac{e_{31}\left(\frac{h}{2} + h_1\right)}{C_v'} \int_{L_1}^{L_2} \frac{\partial^2 w}{\partial x^2} dx, \quad (2-9)$$

when piezoelectric layers/ patches are applied on both surfaces of the host beam:

$$V_a = gV_s = -g \frac{e_{31}(h + h_1)}{2C_v'} \int_{L_1}^{L_2} \frac{d^2w}{dx^2} dx, \quad (2-10)$$

The shear force, S , generated at the interface between the piezoelectric actuator and the host beam can be written as [7, 60]

$$S = \frac{\frac{Ehb_a}{\psi + \alpha} d_{31} V_a}{h_1}, \quad (2-11)$$

where b_a is the width of the piezoelectric actuators, ψ is given as $EH/E_p h_1$, d_{31} is the piezoelectric charge of the piezoelectric layers, and $\alpha = 6$ when the host beam is considered as a bar under bending. A bending moment is hence induced by the shear force at the both ends of the piezoelectric actuator. The bending moment can be obtained by

when piezoelectric layers/ patches are applied on the lower surface of the host beam:

$$M_e = S \frac{h + h_1}{2}, \quad (2-12)$$

when piezoelectric layers/ patches are applied on both surfaces of the host beam:

$$M_e = 2S \left(\frac{h}{2} + h_1 \right). \quad (2-13)$$

It is noteworthy that the exact voltage of the piezoelectric sensors and actuators will not be obtained from the simulations, because the tuning process is eventually applied to each vibration mode shape, which has no definite amplitude, to realize the vibration mode shape tuning. In general, a higher amplitude of free vibration response and a larger curvature at the area covered by the piezoelectric materials lead to a higher voltage output from the piezoelectric sensor. However, no matter what the vibration amplitude and output voltage from the sensor are, the gain factor will be the same.

2.3 Model of a damage

Both the crack and delamination may create discontinuity on the vibration characteristics of the beam. When a crack occurs at the $x=L_c$ of the beam, a slope discontinuity is generated at the crack position given by [41, 61]:

$$\theta = \Theta L w'' \Big|_{x=L_c}, \quad (2-14)$$

where Θ is a function derived from fracture mechanics and Castigliano's theorem [61],

$$\Theta = 6\pi \frac{h}{L} \int_0^{\frac{d}{h}} z \Phi_1(\xi) \left(\frac{0.923 + 1.199 \left(1 - \sin \frac{\pi z}{2} \right)^4}{\cos \left(\frac{\pi z}{2} \right)} \right)^2 \frac{\tan \left(\frac{\pi z}{2} \right)}{\frac{\pi z}{2}} dz, \quad (2-15)$$

where d is the depth of the crack, and $\Phi_1(\xi)$ equals to 1 for isotropic materials.

Rather than generating a slope discontinuity, the delamination separates the delaminated part of the beam into the upper and lower sections. The continuity conditions of the beam are hence altered by the delamination. The boundary conditions and the continuity conditions of the beams with a specific type of damage are discussed in chapter 3, 4 and 5.

3. Crack detection of beams by a vibration characteristics tuning technique through an optimal design of piezoelectric layers

In this chapter, an advanced technique for crack detection in beam structures using a vibration characteristic tuning procedure is developed by an optimal design of piezoelectric materials to realize increased frequency-shifts in beams to efficiently magnify the crack effect for the detection purpose. The tuning process is developed to diminish the environment effect, while increasing the sensitivity of the damage detection. A theoretical model is developed to reveal the principle of damage detection with the tuning process.

3.1 Theoretical models

In this section, the vibration characteristic tuning process in damage detection based on the vibration natural frequencies and mode shapes is explained. Detailed theoretical models are proposed to calculate the changes in natural frequencies of the beams with and without tuning to demonstrate the applicability of the proposed technique.

Fig. 3-1 shows a flow chart that briefly describes the tuning process for damage detection. The electric charge and voltage on the piezoelectric sensor that is proportional to the overall curvature in the area covered by the sensor is obtained first for the feedback process. Then, the piezoelectric actuator is used to generate a feedback bending moment to the host beam based on the voltage from the sensor thereby changing the local stiffness of the beam section covered by the piezoelectric actuator. With different gains applied to the voltage from the sensor, variable size and location of the piezoelectric actuator, the vibration mode shapes of the beam are hence altered to achieve a tuning purpose.

By the vibration characteristic tuning process illustrated by Fig. 3-1, the effect of damage occurrence on the change of the vibration characteristics including vibration mode shapes and natural frequencies will be significantly enhanced, leading to a better damage detection compared with the one without tuning.

To describe the vibration characteristic tuning process, two beams attached with piezoelectric layers are prepared as shown in Fig. 3-2, of which one is intact and the other is damaged. A pair of piezoelectric layers composed of both piezoelectric sensor and actuator layers are bonded on the upper and lower surfaces of the host beam. The poling directions of the piezoelectric sensor and actuator are the same. The piezoelectric layers are assumed to be perfectly bounded to the beam. For engineering structures, most of the damages (e.g., the welding defect because of the strain concentration at the heat affect zone) appear at the joint positions, and most of the joint positions are known in advance. In this paper, it is assumed that the crack is located at the fixed end of the beam to show the effectiveness of the proposed technique first. In Fig. 3-2, L denotes the length of the host beam, and L_1 and L_2 are the distances from the fixed end to the left and right ends of the piezoelectric layers, respectively, h is the height of the host beam, and h_l is the thickness of the piezoelectric layers.

As indicated in Fig. 3-2, the beam is separated into three sections, and only the 2nd section of the beam is covered by piezoelectric layer. The equations of motion for the beam in vibration can be derived from Eq. (2-1) as

$$\begin{aligned}
EI \frac{\partial^4 w_1(x,t)}{\partial x^4} + \rho b h \frac{\partial^2 w_1(x,t)}{\partial t^2} &= 0; \quad 0 < x < L_1 \\
(EI + E_p I_p) \frac{\partial^4 w_2(x,t)}{\partial x^4} + (\rho b h + 2\rho_p b h_1) \frac{\partial^2 w_2(x,t)}{\partial t^2} &= 0; \quad L_1 < x < L_2, \\
EI \frac{\partial^4 w_3(x,t)}{\partial x^4} + \rho b h \frac{\partial^2 w_3(x,t)}{\partial t^2} &= 0; \quad L_2 < x < L
\end{aligned} \tag{3-1}$$

where E and E_p are the Young's modulus of the host beam and the piezoelectric layer, respectively; ρ and ρ_p are the densities of the host beam and piezoelectric layer, respectively; b is the width of the host beam and the piezoelectric layer; I is the moment of inertia of the host beam ($I = \frac{bh^3}{12}$); I_p is the moment of inertia of the piezoelectric layers ($I_p = hbh_1(h/2 + h_1)$); and $w(x, t)$ is the displacement of the beam in the transverse direction.

In this case, the vibration mode shape functions of the three beam sections can be obtained from Eq. (2-2) [7, 62]:

$$\begin{aligned}
W_1(x) &= C_1 \cos \beta_1 x + C_2 \sin \beta_1 x + C_3 \cosh \beta_1 x + C_4 \sinh \beta_1 x & 0 \leq x \leq L_1, \\
W_2(x) &= C_5 \cos \beta_2 x + C_6 \sin \beta_2 x + C_7 \cosh \beta_2 x + C_8 \sinh \beta_2 x & L_1 \leq x \leq L_2, \\
W_3(x) &= C_9 \cos \beta_1 x + C_{10} \sin \beta_1 x + C_{11} \cosh \beta_1 x + C_{12} \sinh \beta_1 x & L_2 \leq x \leq L,
\end{aligned} \tag{3-2}$$

where C_{1-12} are the natural constants, β_1 and β_2 are real constants related with the natural

frequency of the beam ($\beta_1 = \sqrt[4]{\omega^2 \frac{\rho b h}{EI}}$; $\beta_2 = \sqrt[4]{\omega^2 \frac{\rho b h + 2\rho_p b h_1}{EI + E_p I_p}}$), and ω is the natural frequency

of the beam.

For the piezoelectric coupled cracked cantilevered beam, its four boundary conditions and eight continuity conditions [41] can be given as follows:

$$\begin{aligned}
x = 0 : w_1 = 0, \quad \frac{\partial w_1}{\partial x} = 0 \quad (\text{without crack}); \\
x = 0 : w_1 = 0, \quad \frac{\partial w_1}{\partial x} = \theta \quad (\text{with crack}); \\
x = L_1 : w_1 = w_2, \quad \frac{\partial w_1}{\partial x} = \frac{\partial w_2}{\partial x}, \\
EI \frac{\partial^2 w_1}{\partial x^2} + 2 \cdot Me = (EI + E_p I_p) \frac{\partial^2 w_2}{\partial x^2}, \quad EI \frac{\partial^3 w_1}{\partial x^3} = (EI + E_p I_p) \frac{\partial^3 w_2}{\partial x^3}; \\
x = L_2 : w_2 = w_3, \quad \frac{\partial w_2}{\partial x} = \frac{\partial w_3}{\partial x}, \\
(EI + E_p I_p) \frac{\partial^2 w_2}{\partial x^2} = EI \frac{\partial^2 w_3}{\partial x^2} + 2 \cdot Me, \quad (EI + E_p I_p) \frac{\partial^3 w_2}{\partial x^3} = EI \frac{\partial^3 w_3}{\partial x^3}; \\
x = L : \frac{\partial^2 w_3}{\partial x^2} = 0, \quad \frac{\partial^3 w_3}{\partial x^3} = 0.
\end{aligned} \tag{3-3}$$

From the preceding eigen-value problem with numerical calculations on Matlab, the n th natural frequencies of the piezoelectric coupled beam with and without crack, $\omega'_{n,h}$ and $\omega'_{n,d}$ ($n=1, 2, 3, \dots, \infty$), and the associated n th vibration mode can be solved.

To verify the effectiveness of the proposed technique on damage detection at other locations of the structure, another simulation is conducted, assuming that the crack occurs at the middle of the beam ($L_c=0.5\text{m}$) with the same dimensions given in Table 3-1. Instead of putting a piezoelectric patch at the middle of the beam along its length direction, two pairs of piezoelectric patches are attached each from the fixed end to $L_1'=0.495\text{m}$ and from $L_2'=0.505\text{m}$ to the free end. In this case, the beam is separated into 4 sections as shown in Fig. 3-3. Thus, the equations of motion become

$$\begin{aligned}
(EI + E_p I_p) \frac{\partial^4 w_1(x,t)}{\partial x^4} + (\rho b h + 2\rho_p b h_1) \frac{\partial^2 w_1(x,t)}{\partial t^2} &= 0; \quad 0 < x < L_1 \\
EI \frac{\partial^4 w_2(x,t)}{\partial x^4} + \rho b h \frac{\partial^2 w_2(x,t)}{\partial t^2} &= 0; \quad L_1 < x < L_c \\
EI \frac{\partial^4 w_3(x,t)}{\partial x^4} + \rho b h \frac{\partial^2 w_3(x,t)}{\partial t^2} &= 0; \quad L_c < x < L_2 \\
(EI + E_p I_p) \frac{\partial^4 w_4(x,t)}{\partial x^4} + (\rho b h + 2\rho_p b h_1) \frac{\partial^2 w_4(x,t)}{\partial t^2} &= 0; \quad L_2 < x < L.
\end{aligned} \tag{3-6}$$

Accordingly, the boundary conditions and continuous conditions are given as

$$\begin{aligned}
x = 0 : w_1 = 0, \quad \frac{\partial w_1}{\partial x} = 0; \\
x = L_1 : w_1 = w_2, \quad \frac{\partial w_1}{\partial x} = \frac{\partial w_2}{\partial x}, \\
(EI + E_p I_p) \frac{\partial^2 w_1}{\partial x^2} = EI \frac{\partial^2 w_2}{\partial x^2} + 2 \cdot Me, \quad (EI + E_p I_p) \frac{\partial^3 w_1}{\partial x^3} = EI \frac{\partial^3 w_2}{\partial x^3}; \\
x = L_c : w_2 = w_3, \quad \frac{\partial w_2}{\partial x} = \frac{\partial w_3}{\partial x} \text{ (without crack)}, \quad \frac{\partial w_2}{\partial x} + \theta = \frac{\partial w_3}{\partial x} \text{ (with crack)} \\
EI \frac{\partial^2 w_2}{\partial x^2} = EI \frac{\partial^2 w_3}{\partial x^2}, \quad EI \frac{\partial^3 w_2}{\partial x^3} = EI \frac{\partial^3 w_3}{\partial x^3}; \\
x = L_2 : w_3 = w_4, \quad \frac{\partial w_3}{\partial x} = \frac{\partial w_4}{\partial x}, \\
EI \frac{\partial^2 w_3}{\partial x^2} + 2 \cdot Me = (EI + E_p I_p) \frac{\partial^2 w_4}{\partial x^2}, \quad EI \frac{\partial^3 w_3}{\partial x^3} = (EI + E_p I_p) \frac{\partial^3 w_4}{\partial x^3}; \\
x = L : (EI + E_p I_p) \frac{\partial^2 w_4}{\partial x^2} = 2 \cdot Me, \quad (EI + E_p I_p) \frac{\partial^3 w_4}{\partial x^3} = 0.
\end{aligned} \tag{3-7}$$

By the same calculation process, the change of the natural frequencies due to existence of the middle crack can be obtained by the vibration tuning using the piezoelectric patches.

It is noted that, when the feedback gain, g , is set as zero, the beam is considered to have no tuning effect. The tuning with certain feedback gain ($g > 0$) is supposed to lead to better damage detection effect via tuning of the vibration characteristics of the beam. Detailed results comparing the damage detection effects with and without tuning will be given in the following section.

3.2 Simulations and discussions

Numerical simulations based on the proposed theoretical approach are presented in this section. The improvement in damage detection sensitivity is achieved by the active vibration characteristic tuning. Table 3-1 lists the material properties and geometry of the cracked beams with the piezoelectric layers that are used in the simulation.

Table 3-2 shows the results of the changes in natural frequencies of the beam without the tuning process when the feedback gain, g , is set to be zero, with a crack located at the fixed end of the beam. The depth of the crack is 0.004 m, which is 40 % of the thickness of the host beam ($d=0.004\text{m}$). It can be seen that the largest change in natural frequencies occurs in the 1st natural frequency. Therefore, the results for the 1st natural frequency are considered for the case when the crack is at the fixed end. From Table 3-2, it is also noted that the changes in the 1st natural frequency is only 3.37 %, even if the crack is located at the fixed end of the cantilever. Such a sensitivity cannot satisfy the damage detection requirements with inevitable noises.

Fig. 3-4 shows the percent difference of the 1st natural frequency between the intact and cracked beams with the same tuning process and piezoelectric effect for $L_1=0.02\text{m}$ and $L_2=0.81\text{m}$. With an increase in the gain factor from 0 to 40, the change in the 1st natural frequency rises rapidly from 4 to 10 %. Then, the change in the natural frequency grows slowly to 10.5 % when the gain factor increases from 40 to 160. With the increment of the gain factor larger than 160, the local stiffness of the beam section covered by the piezoelectric actuator keeps increasing, but the effect of the local stiffness growth on the damage detection sensitivity enhancement is no longer significant. From Fig. 3-4, it is concluded that the vibration characteristic tuning with a proper gain factor leads to better damage detection as the natural frequency change becomes more significant.

In addition, the geometric properties of the piezoelectric layers are studied and optimally defined to reveal the influence of the location and size of the piezoelectric layers on the detection sensitivity. To achieve a higher detection sensitivity, the largest curvature of the mode shape is supposed to be at the crack position, which will magnify the changes in associated natural frequencies due to the crack existence. Fig. 3-5 shows the relationship between the change in the 1st natural frequency due to the crack occurrence and the location of the piezoelectric layer with the same tuning process ($g=160$). The length of the piezoelectric layer is 0.79 m, and a fixed gain factor, $g=160$, is applied. It is seen that the change in natural frequency induced by the crack increases from 4.5 to 12.3 %, when the position of the left end of the piezoelectric layers, L_1 , moves from 0.185 to 0.005 m. The effect of the crack existence on the change in natural frequency becomes more significant when the piezoelectric layers get closer to the crack position. In consideration of the installation of the piezoelectric layers, L_1 is defined as 0.01 m rather than the exact fixed end of the cantilever. Furthermore, to find out the optimal size of the piezoelectric layers, simulations with 6 different values of L_2 are conducted, while L_1 is fixed at 0.01 m. Fig. 3-6 shows the change in the 1st natural frequency due to the crack existence versus the length of the piezoelectric layers, when the location of the piezoelectric layer and the gain factor are fixed at $L_1=0.01$ m and $g=160$, respectively. The result reveals that, while the length of the piezoelectric layer, $L_2- L_1$, is altered from 0.29 to 0.49 m, the change in the 1st natural frequency surges from 11 to 18%. Then the frequency change due to the crack existence drops to 11.5 %, when the length $L_2- L_1$ increases to 0.49 from 0.79 m. Clearly, the optimal length of the piezoelectric layer leading to the most significant frequency change (18 %) in the presence of the crack through the tuning process is $L_2=0.5$ m.

By the optimal design of the piezoelectric layers, another simulation of the cantilevered beam with a small crack ($a=0.002$ m, 20% of the thickness of the beam) at the fixed end is studied. As shown

in Fig. 3-7, the change in the 1st natural frequency is lower than 1 % for the case with no vibration tuning. After imposing the vibration tuning on the beam, the change of 1st natural frequency is up to 5.6 % when the gain factor is larger than 160. Consequently, the effectiveness of the proposed technique in detecting small damages is verified.

When the crack is located at the middle of the cantilevered beam, the piezoelectric patches are placed close to the crack, from the fixed end of the beam to L_1' , and from L_2' to the free end of the beam. Fig. 3-8 shows the difference of the 1st and 2nd frequencies between the intact and cracked beams with vibration tuning. It is seen that when the gain factor changes from 0 to 200, the changes in the 1st and 2nd natural frequencies due to the crack existence are increased from 0.50 and 2.16 % to 3.61 and 9.5 %, respectively. Clearly, the damage detection sensitivity is significantly enhanced by the vibration characteristic tuning process, even when the crack is located at the middle of the beam. The variation of the 2nd natural frequency shows a clearer detection result, since the largest curvature is distributed closer to the crack position in the 2nd vibration mode shape of the beam.

3.3 Summary

An optimally designed vibration characteristic tuning technique is presented to greatly improve the sensitivity of damage detection based on the changes in natural frequencies. The bending moments induced by the inverse piezoelectric effect of the piezoelectric actuators are utilized to tune the vibration natural frequencies and mode shapes so as to magnify the changes in the natural frequencies due to the damage existence. A theoretical model is developed to reveal the basic principle of sensitivity enhancement of the proposed damage detection technique. With an optimal design of the piezoelectric sensors and actuators with the dimension of $L_1=0.01\text{m}$ and $L_2=0.5\text{m}$, the changes in the 1st natural frequency due to the damage existence is found to increase from 3.3 to 18 % under the same tuning process with a gain factor of 160 by numerical simulations. The

technique is also found to be efficient for detecting the crack located at different positions of the beam with proper placement of the piezoelectric sensors and actuators. Overall, the vibration characteristic tuning crack detection is promising for the structural health monitoring with an increased sensitivity than the traditional methods with no tuning.

Table 3-1 Geometric and material properties for numerical simulations

Parameter	Host beam (aluminum)	Piezoelectric layers
Young's modulus (N m⁻²)	$E=69\times 10^9$	$E_p=78\times 10^9$
Mass density (kg m⁻³)	$\rho=2.8\times 10^3$	$\rho_p=7.5\times 10^3$
e_{31} (C/m²)	-	-2.8
d_{31} (C/N)	-	-1.28×10^{-10}
C_v (nF)	-	2.633 for a piezoelectric patch with dimensions of 0.01m×0.79m×0.0003m
L (m)	1	-
L_1 (m)	0.01, 0.03, 0.05	-
L_2 (m)	0.3, 0.4, ..., 0.8	-
L_1' (m)	0.495	-
L_2' (m)	0.505	-
L_c (m)	0, 0.5	-
h (m)	0.01	-
h_l (m)	-	0.0003
b (m)	0.02	-
b_s (m)	-	0.01
b_a (m)	-	0.01
d (m)	0.004	-

Table 3-2 Difference in natural frequencies for healthy and cracked beams in traditional method

	1 st order	2 nd order	3 rd order
Healthy beam (Hz)	8.02	50.26	140.72
Cracked beam (Hz)	7.75	48.61	136.33
Percentage of variation (%)	3.37	3.29	3.12

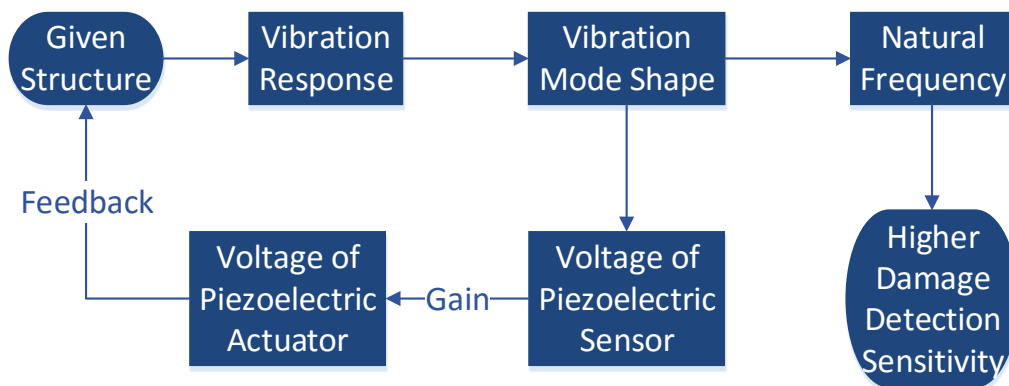


Fig. 3-1 Procedure of vibration characteristic tuning.

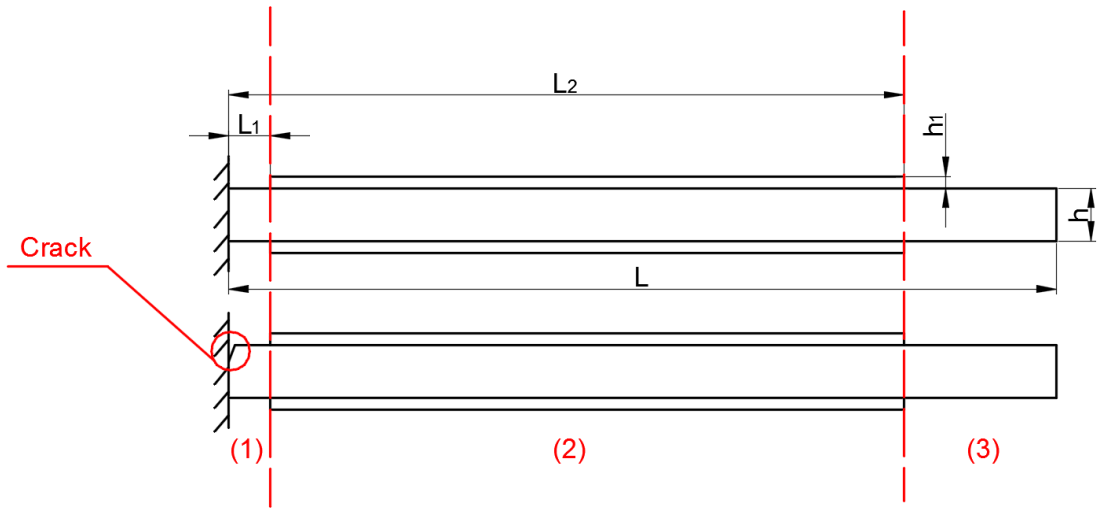


Fig. 3-2 Cantilevered beams with and without a crack at the fixed end.

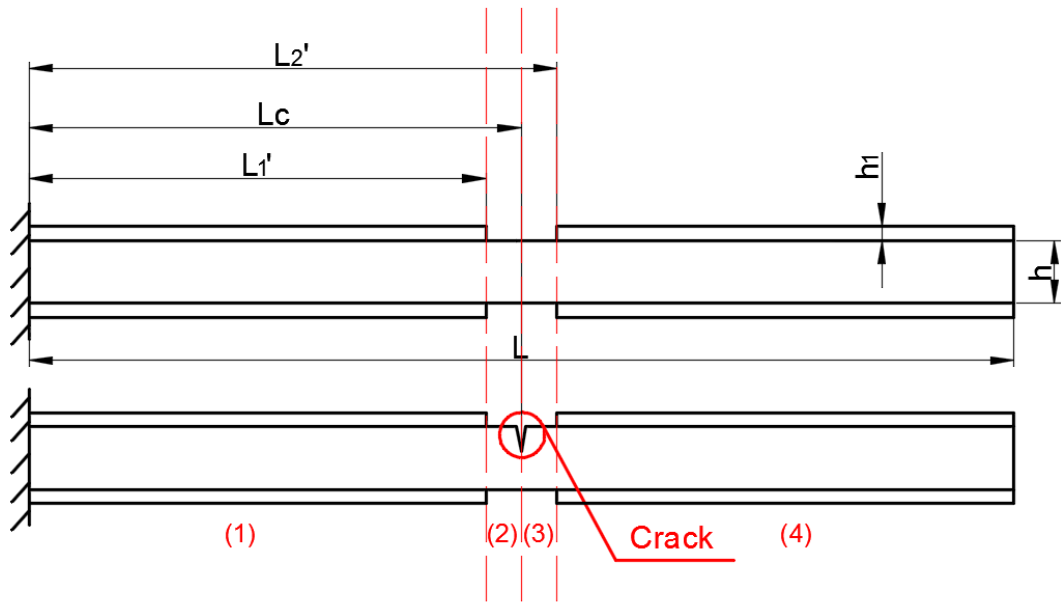


Fig. 3-3 Cantilevered beams with and without a crack at the middle.

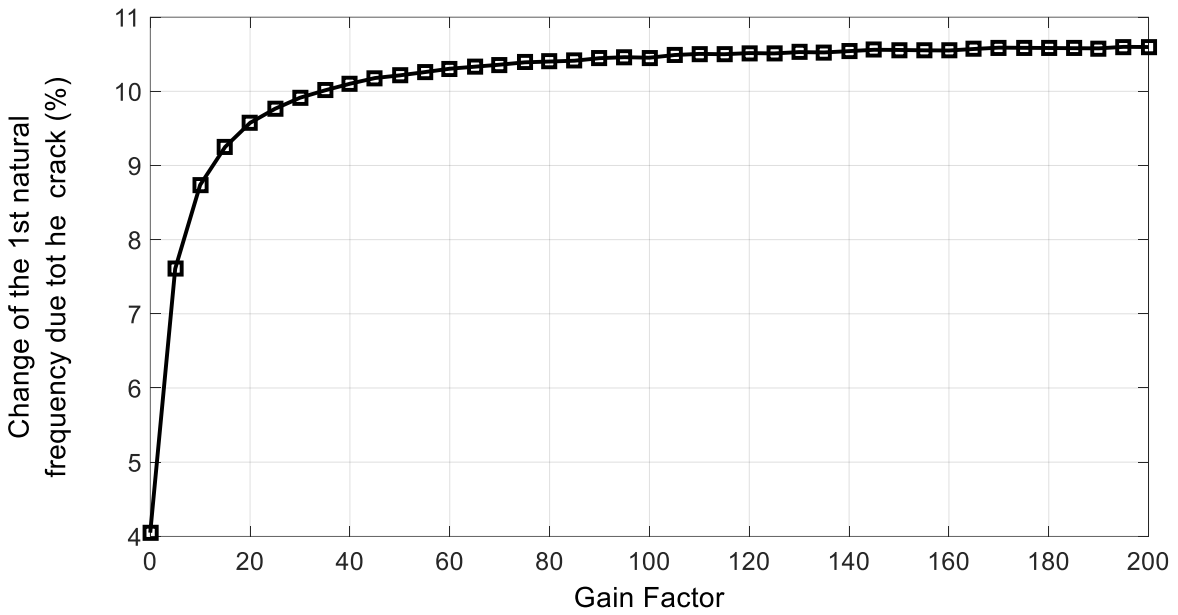


Fig. 3-4 Difference of the 1st natural frequency between the cracked and intact beams with vibration characteristic tuning versus gain factor for $d=0.004\text{m}$, $L_1=0.02\text{m}$ and $L_2 =0.81\text{m}$.

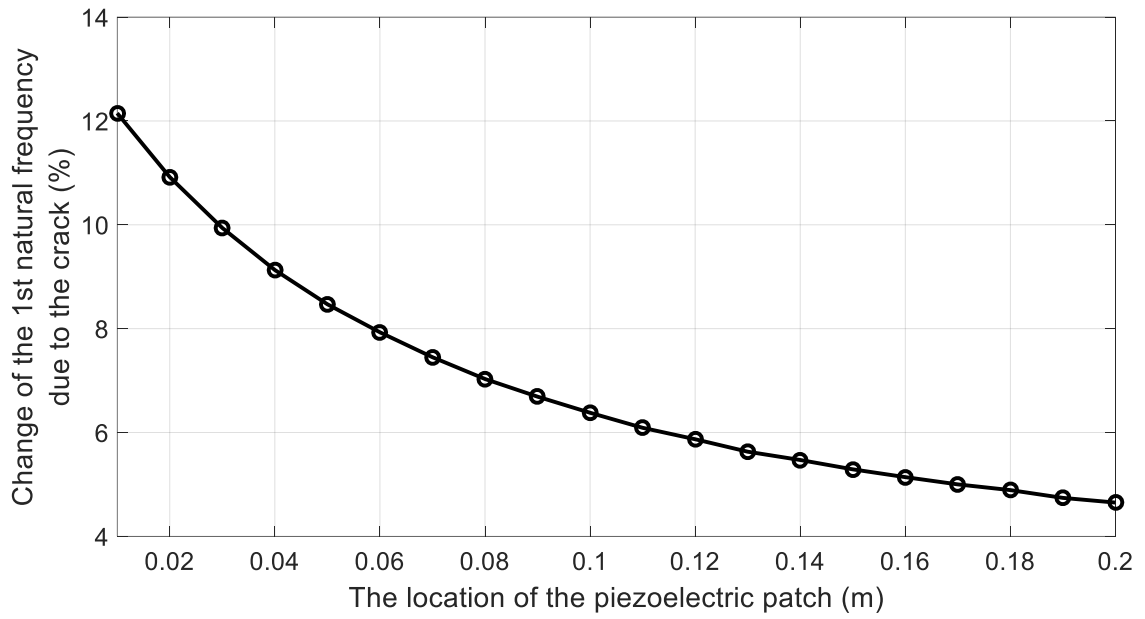


Fig. 3-5 Variation in 1st nature frequency due to a crack ($d=0.004\text{m}$) versus location of the piezoelectric layer with certain length, $L_2-L_1=0.79\text{ m}$, and a fixed gain factor, $g=160$.

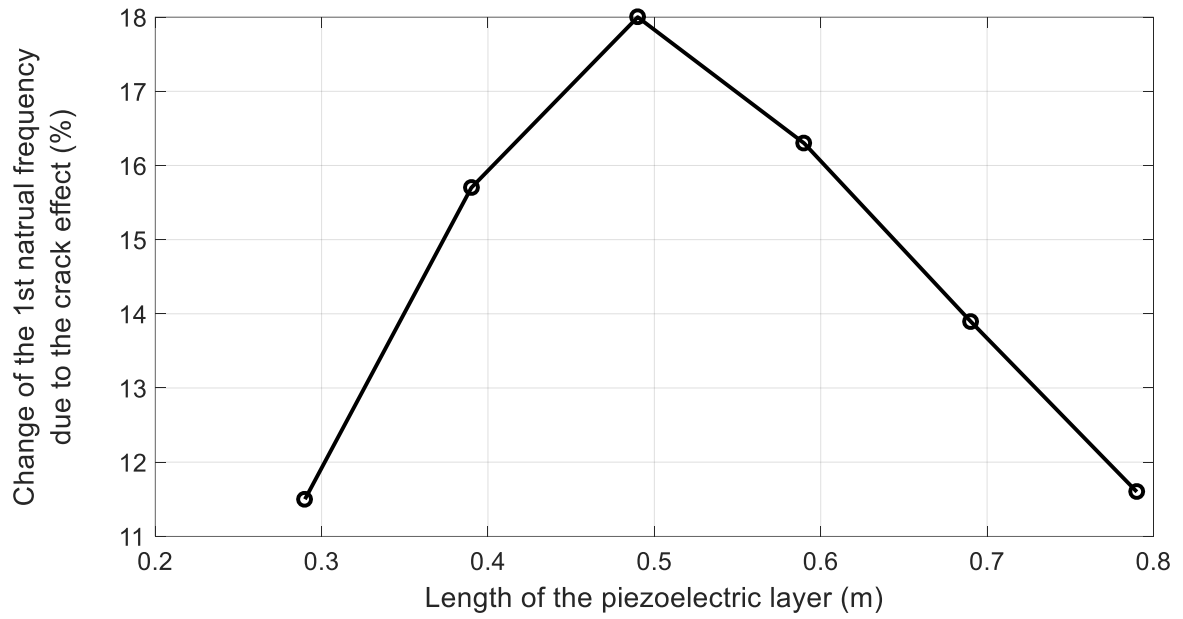


Fig. 3-6 Change in 1st nature frequency due to a crack ($d=0.004\text{m}$) versus length of the piezoelectric layer located at a fixed location, $L_I=0.01\text{m}$, with a fixed gain factor, $g=160$.

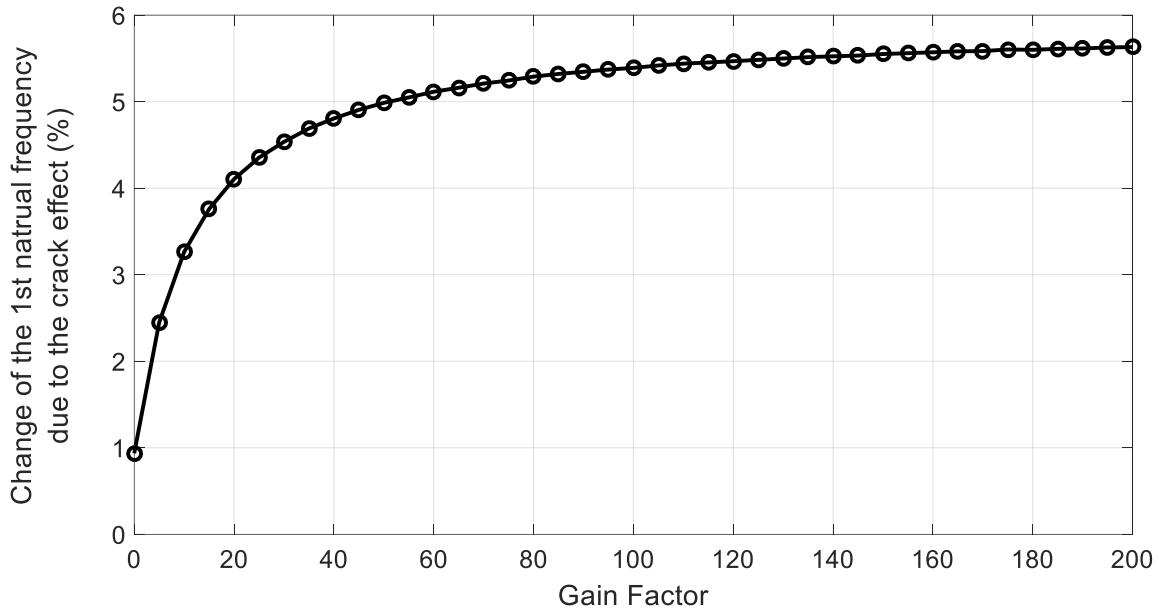


Fig. 3-7 Difference in the 1st natural frequency between cracked and intact beams with vibration characteristic tuning versus gain factor for $d=0.002\text{m}$, $L_1=0.005\text{m}$ and $L_2=0.5\text{m}$.

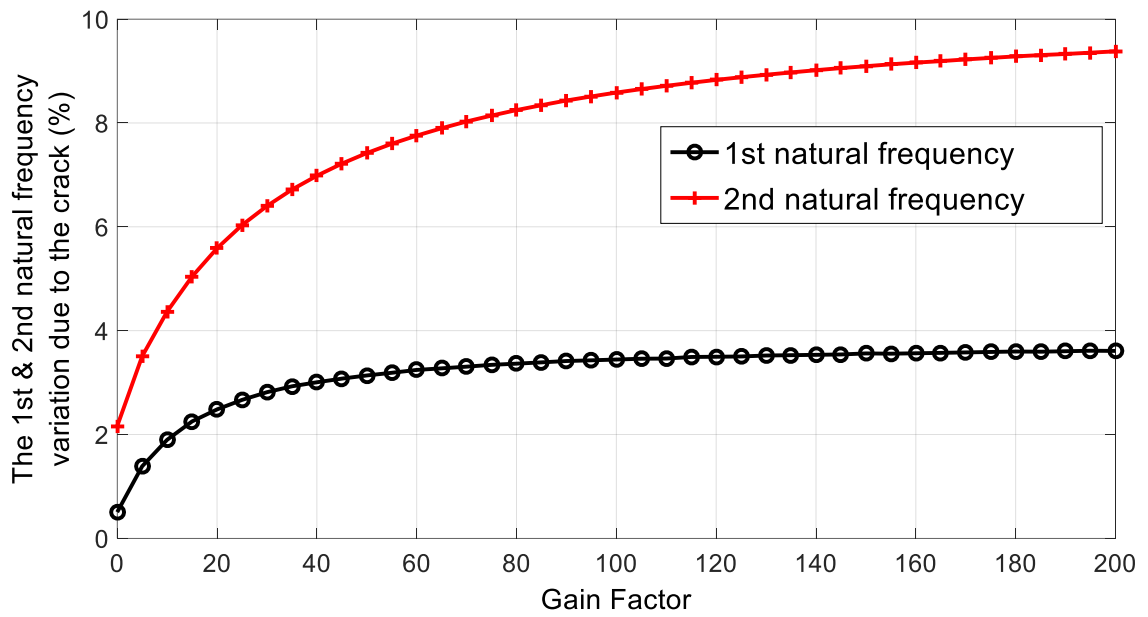


Fig. 3-8 Changes in 1st and 2nd natural frequency due to a crack at the midspan for different gain factors.

4. Crack identification through a scan-tuning process using piezoelectric materials

In this chapter, a scan vibration tuning methodology is proposed for crack damage identification in beam-type structures, including the steps of detection and localization. This methodology resolves the shortcoming of low sensitivity measurement of natural frequencies based damage detection methods by utilizing the merits of active feedback control by means of the piezoelectric materials. Piezoelectric sensors and actuators are mounted on the surface of the host beam synchronously to generate the feedback bending excitations by applying certain gain on the voltage output from the piezoelectric sensors. The stiffness of the original beam is adjusted by the feedback excitations, and the mode shapes and natural frequencies are tuned accordingly. To fulfill the scan-tuning process, each pair of sensor and actuator is activated and controlled individually one by one. When the piezoelectric actuator at the crack position is activated, and the ones at other positions are shut off, the mode shapes of the beam is supposed to be noticeably altered along with the change of its natural frequency due to the crack occurrence. Through the scan-tuning process by activating the piezoelectric actuator at different positions and adjusting the gain, the crack existence and location can be learned from the measured natural frequencies change compared with the healthy beam. A finite element model is established to verify the effectiveness of the proposed methodology.

4.1 Theoretical model

In this section, the scan-tuning process of the proposed methodology for crack identification by measuring the vibration natural frequency change is first explained. Detailed theoretical models are subsequently developed to calculate the changes in natural frequencies of the beam due to the crack with and without the vibration tuning, respectively.

As shown in Fig. 4-1, the crack identification methodology is realized through a scan vibration tuning process. The coefficients, g and n , are defined at the beginning, while g is the gain applied to the voltage output of the sensor, and the amplified voltage will be imposed on the actuator to realize the feedback excitation. n indicates that the n th couple of piezoelectric sensor and actuator from the fixed end of the cantilever beam is subjected to the feedback tuning. To realize the scan-tuning on a whole beam, n is usually set to start as 1. The couples of piezoelectric patches are then activated one by one to generate feedback bending moments at different locations of the beams. When the bending moment is applied at the position where the crack occurs, the local stiffness of the beam is supposed to be noticeably altered through the feedback tuning process, which leads to more significant change on the natural frequencies of the beam—due to the crack [63, 64]. Therefore, the crack can be detected and localized at the same time by comparing the natural frequencies, when the feedback bending moment is applied at different locations of the beams through the scan vibration tuning process. The severity of the crack can be also learned from the amount of the natural frequency change through numerical simulations.

To describe the scan vibration tuning process, a cracked cantilever beam coupled with piezoelectric materials is prepared as shown in Fig. 4-2, with the total length L , width b , thickness H , density ρ and Young's modulus E . Piezoelectric sensor and actuator patches are bonded in pairs on the lower surface of the host beam to realize the feedback vibration tuning. Each piezoelectric

patch has the same length a , thickness h_l , density ρ_p and Young's modulus E_p . b_s and b_a are the width of the piezoelectric sensor and actuator, respectively. A healthy beam with the same dimensions and material properties is also provided for the comparison with the cracked one. It is noted that the poling direction of the piezoelectric sensor is opposite to the one of piezoelectric actuator.

According to Eq. (2-1), the dynamic equation of the beam fully covered by piezoelectric sensor and actuator patches can be written as

$$(EI)' \frac{\partial^4 w(x,t)}{\partial x^4} + m' \frac{\partial^2 w(x,t)}{\partial t^2} = 0, \quad (4-1)$$

where $w(x,t)$ is the dynamic vibration deflection of the beam. m' and $(EI)'$ are the equivalent mass and the flexural rigidity of the cantilever covered by piezoelectric patches given by

$$\begin{aligned} m' &= \rho h b + \rho_p h_l (b_s + b_a), \\ (EI)' &= E \left(\frac{(h-h_1)^3 + (h+h_1)^3}{24} \right) b + E_p \left(\frac{(h-h_1)^3 - (h+h_1)^3}{24} \right) (b_s + b_a), \end{aligned} \quad (4-2)$$

As shown from Fig. 4-2, the crack is located at the position with L_c away from the fixed end of the beam. The feedback voltage is applied to the piezoelectric actuator individually from the fixed end to the free end of the beam to altered its local stiffness at different locations and realize the scan tuning process. Hence, only one pair of piezoelectric patches are activated each time, and the cracked beam is simply separated into 4 sections by the activated piezoelectric sensor and actuator pair and the position of the crack. The modelling process of the healthy beam is the same, while the crack depth is regarded as zero. Depending on Eq. (2-2), the mode shape functions of the 4 beam sections, $W_i(x)$, are given by ($1 \leq i \leq 4$)

$$\begin{aligned}
W_1(x) &= C_1 \cos \beta x + C_2 \sin \beta x + C_3 \cosh \beta x + C_4 \sinh \beta x & 0 \leq x < L_a, \\
W_2(x) &= C_5 \cos \beta x + C_6 \sin \beta x + C_7 \cosh \beta x + C_8 \sinh \beta x & L_a \leq x < L_b, \\
W_3(x) &= C_9 \cos \beta x + C_{10} \sin \beta x + C_{11} \cosh \beta x + C_{12} \sinh \beta x & L_b \leq x < L_c, \\
W_4(x) &= C_{13} \cos \beta x + C_{14} \sin \beta x + C_{15} \cosh \beta x + C_{16} \sinh \beta x & L_c \leq x \leq L,
\end{aligned} \tag{4-3}$$

where C_{1-16} are the unknown constants, β is real constant related with the natural frequency of the

structure given by $\beta = \sqrt[4]{\omega^2 \frac{m'}{(EI)'}}$, ω is the natural frequency of the beam, L_1 and L_2 are the

distance from the fixed end of the beam to the left and right ends of the activated piezoelectric actuator, respectively. L_a , L_b and L_c are the positions along the length direction of the beam.

Depending on the placement of the active piezoelectric sensor and actuator patches and the position of the crack, the definitions of L_a , L_b and L_c are listed in Table 4-1.

The boundary conditions and continuity conditions of the beam coupled with piezoelectric patches are listed in Appendix B. The piezoelectric induced bending moments are imposed into the continuity conditions at both ends of the activated piezoelectric actuators. Substituting Eqs. (2-2), (2-13), (2-14) and (4-3) into boundary conditions and continuity conditions illustrated by Eqs. (B-1) to (B-3) leads to 16 linear equations, from which the n th natural frequencies of the beam under the vibration tuning, $\omega'_{n,h}$ and $\omega'_{n,d}$ ($n=1, 2, 3, \dots, \infty$), can be solved by the Eigen value problem.

Based on the magnified crack effect on the natural frequencies change through the scan vibration tuning process, the existence and of the crack can be learned. Detailed crack identification results and discussions are given in the next section.

4.2 Numerical simulations and discussions

Numerical Simulations based on the theoretical model are conducted in this section. Damage identification to the crack with different severity located at different locations of the beam is realized by the proposed methodology. Mechanism of the scan vibration tuning techniques are discussed and explained through simulation results. Table 4-2 lists the dimensions and material properties of the host beam and the piezoelectric patches used in the simulations.

Table 4-3 shows the results of the changes in the first three natural frequencies of the beam without the scan-tuning process when the feedback gain, g , is set to be zero, with a crack located at the center of the beam ($x=0.32\text{m}$). The depth of the crack, d , is 0.0012 m , which is 40 % of the thickness of the host beam. However, it is noted that the largest change in the first three natural frequencies (the 2nd natural frequency) is only 0.89 %. Such a sensitivity cannot satisfy the damage detection requirements with inevitable noises. The damage location cannot be learned directly from the natural frequencies change either.

To find a suitable gain for the scan vibration tuning process with better detection sensitivity, the effect of the gain applied to the voltage output of the piezoelectric sensor on the natural frequency change due to the crack is drawn in Fig. 4-3. The gain increases from -8.5 to 8.5, while the crack with depth of 40% of the thickness of the beam ($d=0.0012\text{m}$) is located at $L_c=0.32\text{m}$ (around the middle of the beam). Previous study indicates that higher detection sensitivity can be achieved [63, 64], when the piezoelectric actuator is located closer to the damage. The piezoelectric actuator close to the crack at $L_l=0.32\text{m}$ is hence activated to tune the vibration characteristics of the beam. In Fig. 4-3, it is found that the change in natural frequencies due to the crack becomes even poorer when the gain is negative. With positive gain, it is seen that the gain increment leads to the sensitivity enhancements on damage detection with more obvious changes for all three natural

frequencies. However, this increment of the change of the 3rd natural frequency with the gain increment is less obvious compared with 1st and 2nd one. The reason of this phenomenon is related with the crack location and natural vibration mode shapes and will be explained in the following discussions.

To study the scan vibration tuning for both crack detection and localization, Fig. 4-4 displays the detection results of the change in the first three beam natural frequencies due to the crack, when the piezoelectric actuators located at different positions of the beam are activated. The feedback gain is fixed at 8.5, and the same crack located at the middle of the host beam ($L_c=0.32\text{m}$, $d=0.0012\text{m}$) is used. From Fig. 4-4, it can be found that the percent changes are 22%, 25%, 2% in the first three natural frequencies, respectively, compared with ones of the healthy beam, when the sixth piezoelectric ($L_I=0.31\text{m}$) actuator is activated. When piezoelectric actuators at other locations are activated, the natural frequency changes are not obvious (less than 2%). Figs. 4-5 (a), (b) and (c) show the first three mode shapes of the beam, while the piezoelectric actuators at different locations are activated. It is seen that the vibration tuning changes the natural vibration mode shapes of the beam and enlarges the slope discontinuity at the crack position obviously, when the piezoelectric actuator closed to the crack is activated by the feedback voltage, leading to more obvious natural frequency change and higher crack detection sensitivity. Through the scan vibration tuning process, the crack at any position of the beam can be effectively detected and localized with the notification of obvious natural frequency change. Moreover, for the case of the middle crack of the beam, it is found that the changes of the 1st and 2nd natural frequencies with $L_I=0.31\text{m}$ clearly reveal the existence as well as the location of the damage. However, the change in the 3rd natural frequency is insignificant for damage detection or localization. Similar phenomenon can be found in Fig. 4-5 (c) with insignificant change of the 3rd natural vibration

mode shape even if the piezoelectric actuator close to the crack is active. To explain the difference of detection sensitivity in different modes, the non-dimensional curvature distributions of the first three natural mode shapes of the beam are plotted in Fig. 4-6. It is noted that very small curvature is distributed at the middle of the beam in the 3rd mode, which leads to minor slope difference on both sides of the crack. From Eqs. (2-6), (2-8), (2-10), (2-11) and (2-13), the feedback excitation is proportional to the slope difference between both sides of the piezoelectric sensor. Therefore, even if the piezoelectric actuator patch located at the crack is activated, the feedback excitation corresponding to the 3rd mode is relatively weak due to the lack of slope difference between two sides of the piezoelectric sensor and the small voltage output from the sensor. From the results shown in Figs. 4-4 to 4-6, it can be concluded that the scan vibration tuning process can effectively detect and locate the crack damage by amplify the natural frequencies changes due to the crack, but sensitivity for different natural modes can vary depending on the position of the crack and the mode shapes.

The results of the case when a crack appears close to the fixed end of the cantilever ($L_c=0.05\text{m}$) are then provided in Fig. 4-7. The depth of the crack stays at 40% of the thickness of the host beam ($d=0.0012\text{m}$). In this case, as shown in the Fig. 4-7, the appearance of the crack contributes 24% to the shift of the first natural frequency while the gain is 8. However, the crack effect makes tiny difference to the 2nd and 3rd natural frequencies. As a further illustration for the cases of different locations of the crack, more simulation results are plotted in Fig. 4-8, where the gain is set as $g=8$. The distance between the fixed end of the cantilever beam and the crack (L_c) changes from 0.05m to 0.59m. To show the optimal detection results, only the scan-tuning results with the largest natural frequency changes, when the piezoelectric actuators close to the crack positions are activated, are given. It is found that the 1st natural frequency change of the beam reflects the most

significant crack effect among the first three natural frequencies, when distance between the crack and the fixed end is 0.05m to 0.29m. When the crack is located at 0.29m to 0.47m away from the fixed end, the 2nd natural frequency change is the optimal characteristic for detection. The 3rd natural frequency change is the most effective one for the detection of the crack situated close to the free end of the cantilever beam ($L_c \geq 0.47m$).

The damage identification results for the cases with different crack depth are plotted in Fig. 4-9 to study the effect of the crack size on the detection sensitivity. The crack location and the gain factor are fixed as the former case ($L_c = 0.32m$, $g=8.5$). The piezoelectric actuator close to the crack ($L_l=0.31$) is activated. Corresponding with the increase of the crack depth from 0% to 40% of the beam thickness (0 to 0.0012 m), the changes in the first three natural frequency keep increasing showing the higher detection sensitivity. The sensitivity enhancements in the first three natural frequencies display a similar trend as the ones in Fig. 4-3. Specifically, the change of the 2nd natural frequency shows the most significant sensitivity (up to 25% with 40% crack depth percentage of the beam thickness) in damage identification due to the crack located at the middle of the beam. It can be explained in the same way by looking at Fig. 4-5 (b) and Fig. 4-6 that with large curvature distribution at the middle section of the beam, the feedback excitation and vibration tuning effect corresponding to the 2nd mode is more significant compared with the ones of other modes, which leads to more obvious change in 2nd natural frequency due to the crack and better damage detection sensitivity. From the given simulation results, we can recognize the potential of the crack depth quantification by using the proposed methodology as well. After the crack is located, and the gain is fixed, the crack depth can be learned reversely from the natural frequency change for the damage evaluation aim.

4.3 Finite element method simulations

The scan-tuning crack identification is an improved damage monitoring methodology of the vibration characteristic tuning crack detection. To better verify the effectiveness of the proposed methodology of scan-tuning on beam-type structures, a finite element model is developed on ANSYS 16.0. The dimensions and material properties of the finite element beam model is based on Table 4-2. Beam 188 elements are employed to mesh the cantilever beam model. As shown in Fig. 4-10, A crack located at $x=0.32\text{m}$ is presented by the reduction of the height of the beam section properties. To better reveal the natural frequencies of the beam from the vibration response, two initial forces are applied on the beam at $x=0.298\text{m}$ ($F_{z1}=30\text{N}$) and $x=0.598\text{m}$ ($F_{z2}=-10\text{N}$). The initial forces are deleted after 0.2 seconds ($t=0.2\text{s}$), and the transient analysis of the free vibration of the beam is subsequently initiated. According to Eq. (2-13), a couple of feedback bending moments are imposed on both sides of the activated piezoelectric patches due to the piezoelectric effect. The gain factor, g , during the transient analysis is defined as 8.5 for the comparison with numerical simulations in Matlab. The data of the nodal displacement on z-axis direction is recorded and processed by fast Fourier transform (FFT) to draw the frequency spectrum.

Figs. 4-11 (a) and (b) display the frequency spectrums of both the healthy beam and cracked beam with and without using scan-tuning method. The natural frequencies are extracted and listed in Table 4-4 and Table 4-5, respectively. From Table 4-4, it can be seen that the crack effect is extremely weak in all the three natural frequencies in traditional frequency-based detection method with the highest natural frequency change of only 2.56% for the 2nd vibration mode. On the other hand, as shown in Table 4-5, with the scan-tuning process, the first two natural frequencies of both the healthy beam and the cracked beam are decreased, but the difference in the 1st and 2nd natural frequencies between both beams significantly surges to 20.83% and 24.63% respectively. The

vibration tuning barely changes the 3rd natural frequencies of both beams. The overall results from the transient analysis based on FEM simulations are similar to the ones from numerical simulations, while the 2nd natural frequency is the most sensitive parameter for the detection on the crack at the middle of cantilever beam via scan-tuning method. The effectiveness of the proposed methodology is hence proven by the FEM simulations.

4.4 Summary

A damage identification methodology for beam-type structures by the use of piezoelectric materials is proposed. The piezoelectric sensors and actuators are employed to generate the feedback excitations to change the local stiffness so that to alter the mode shape of the beam. The scan vibration tuning process is realized through the activation of each pair of piezoelectric sensor and piezoelectric actuator individually over the surface of the host beam. By studying the natural frequency change compared with the healthy beam under the same scan-tuning process, the damage in the host beam can be identified. A detailed theoretical model is established to realize the damage identification with the scan vibration tuning, and numerical simulations based on the model are conducted. Cracks at different positions of the beam can be effectively detected and located by the proposed methodology. With the scan-tuning, the crack at the center and the fixed end of the beam can lead up to 25% change in the natural frequencies of the beam. It is also found that the damage detection sensitivity with different natural frequencies and vibration modes could vary depending on the position of the crack and the mode shapes. The damages close to the position with highest curvature of a specific order natural vibration mode shape are easier to be detected with higher sensitivity and more significant natural frequency change. The detection of the crack at certain position but with different depth is also discussed, and the potential of damage

quantification through this methodology is recognized. The damage detection and localization process is also verified to be efficient by the FEM simulations.

Table 4-1 The definition of the L_a , L_b and L_c

Relationship between the locations of the activated actuator and the crack	$L_2 < L_c$	$L_1 \leq L_c \ \& \ L_2 \geq L_c$	$L_1 > L_c$
L_a	L_1	L_1	L_c
L_b	L_2	L_c	L_1
L_c	L_c	L_2	L_2

Table 4-2 Geometric and material properties for numerical simulations

Parameter	Host beam (aluminum)	Piezoelectric patches
Young's modulus (N m^{-2})	$E=69 \times 10^9$	$E_p=78 \times 10^9$
Mass density (kg m^{-3})	$\rho=2.8 \times 10^3$	$\rho_p=7.5 \times 10^3$
e_{31} (C m^{-2})	-	-2.8
d_{31} (C N^{-1})	-	-1.28×10^{-10}
C_v (nF)	-	0.643 for a piezoelectric patch with dimensions of $0.01\text{m} \times 0.06\text{m} \times 0.00035\text{m}$
L (m)	0.62	-
L_1 (m)	0.01, 0.07, ..., 0.55	-
L_2 (m)	$L_1 + l_p$	-
L_c (m)	0.05, 0.32	-
h (m)	0.003	-
h_1 (m)	-	0.00035
b (m)	0.02	-
b_s (m)	-	0.01
b_a (m)	-	0.01
d (m)	0 (healthy beam) 0.0012 (damaged beam)	-
l_p (m)	-	0.06

Table 4-3 Difference in natural frequencies for healthy and cracked beams ($L_c=0.32\text{m}$,
 $d=0.012\text{m}$)

	1st order	2nd order	3rd order
Healthy beam (Hz)	6.56	41.06	114.97
Cracked beam (Hz)	6.54	40.70	114.94
Percentage of variation (%)	0.24	0.89	0.03

Table 4-4 Difference in natural frequencies of healthy and cracked beams in FEM simulation
without vibration tuning

	1st order	2nd order	3rd order
Healthy beam (Hz)	6.25	39.00	105.5
Cracked beam (Hz)	6.25	38.00	105.25
Percentage of variation (%)	0	2.56	0.24

Table 4-5 Difference in natural frequencies of healthy and cracked beams in FEM simulation
with vibration tuning at appropriate position

	1st order	2nd order	3rd order
Healthy beam (Hz)	6.00	33.50	106.00
Cracked beam (Hz)	4.75	24.25	105.5
Percentage of variation (%)	20.83	24.63	0.47

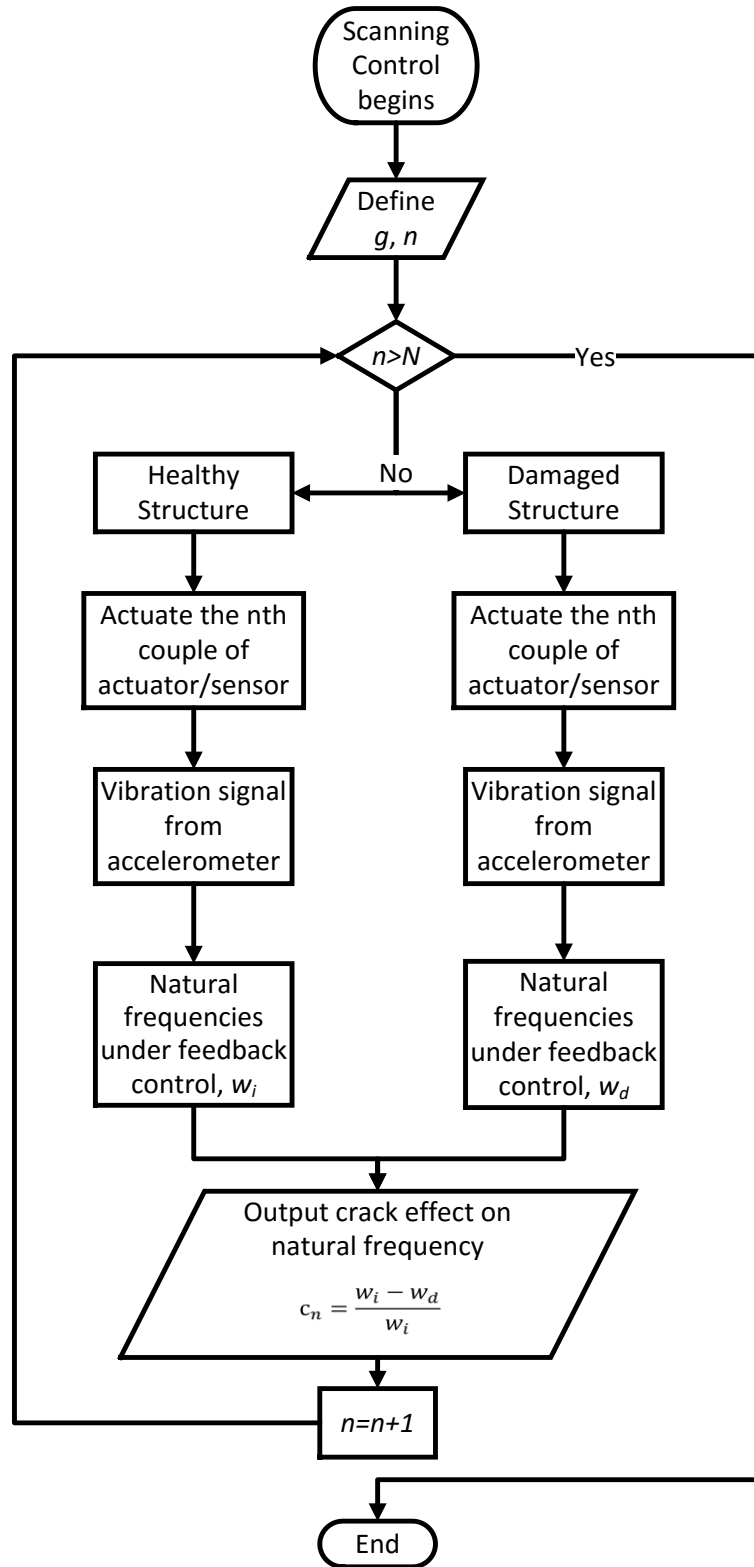


Fig. 4-1 Procedure of scan vibration tuning method.

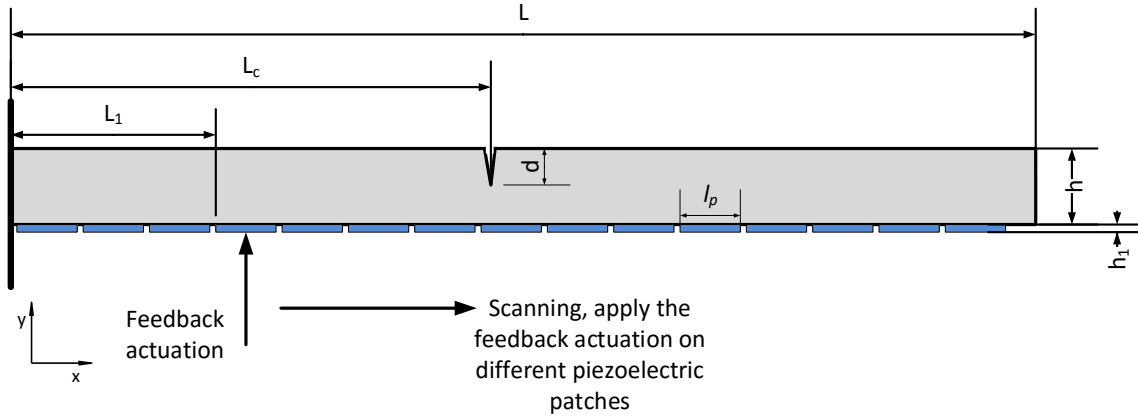


Fig. 4-2 Physical model of a cracked cantilever beam coupled with piezoelectric patches.

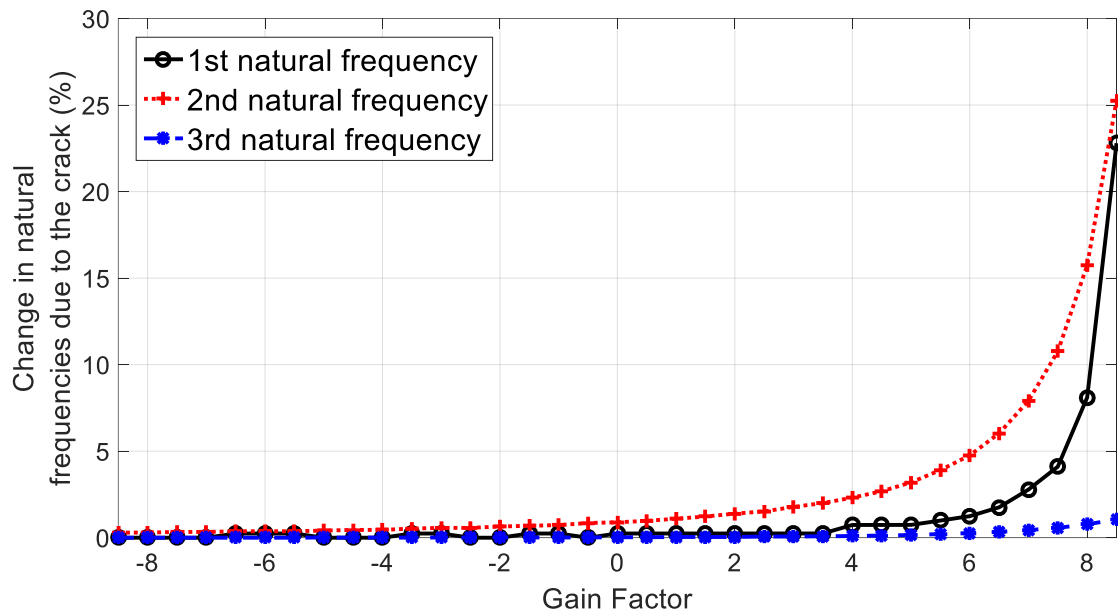


Fig. 4-3 The change in the natural frequencies of the cantilever beam due to the crack effect with different gain under the scan-tuning, where the values for $L_c=0.32$ m, $L_1=0.31$ m, $d=0.0012$ m.

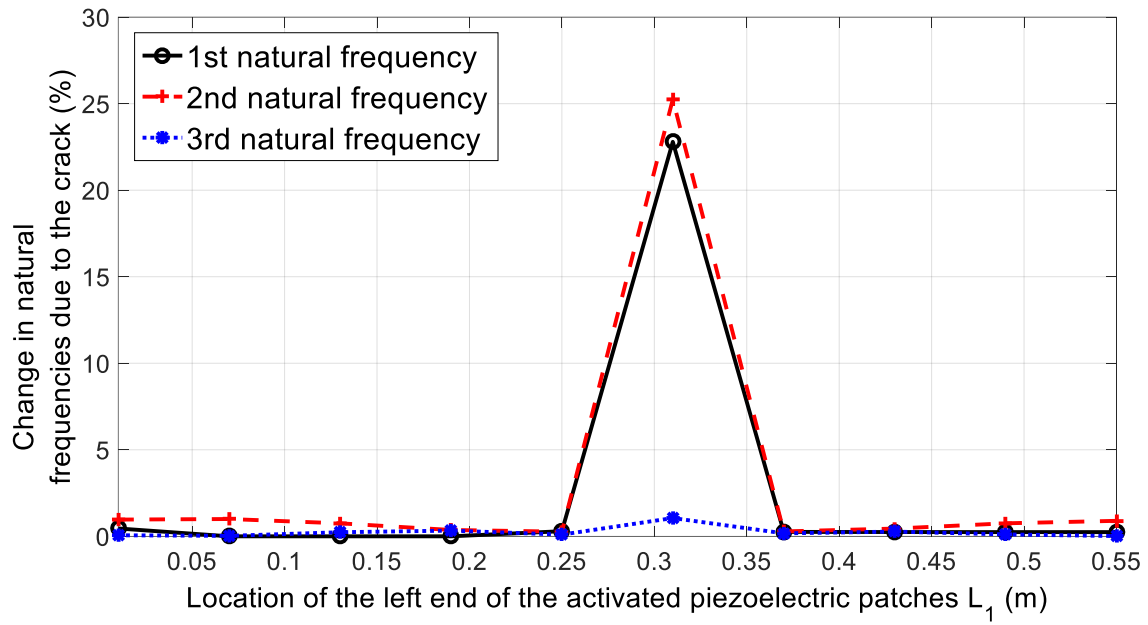


Fig. 4-4 The change in the natural frequencies of the cantilever beam due to the crack effect under the scan-tuning, where the values for $L_c=0.32$ m, $d=0.0012$ m and $g=8.5$.

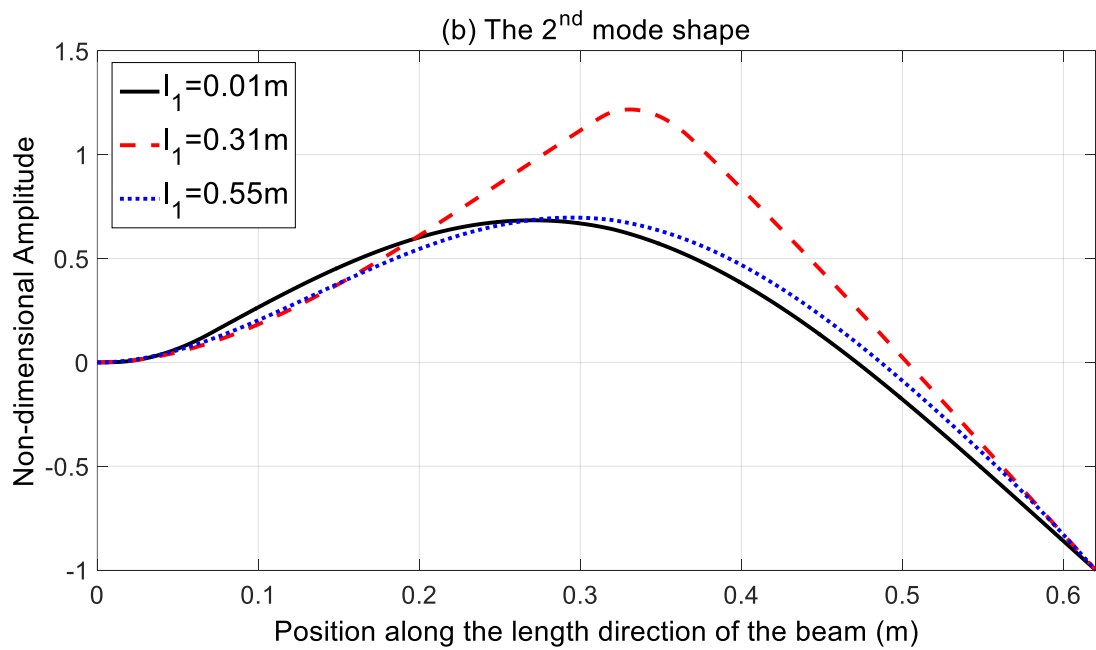
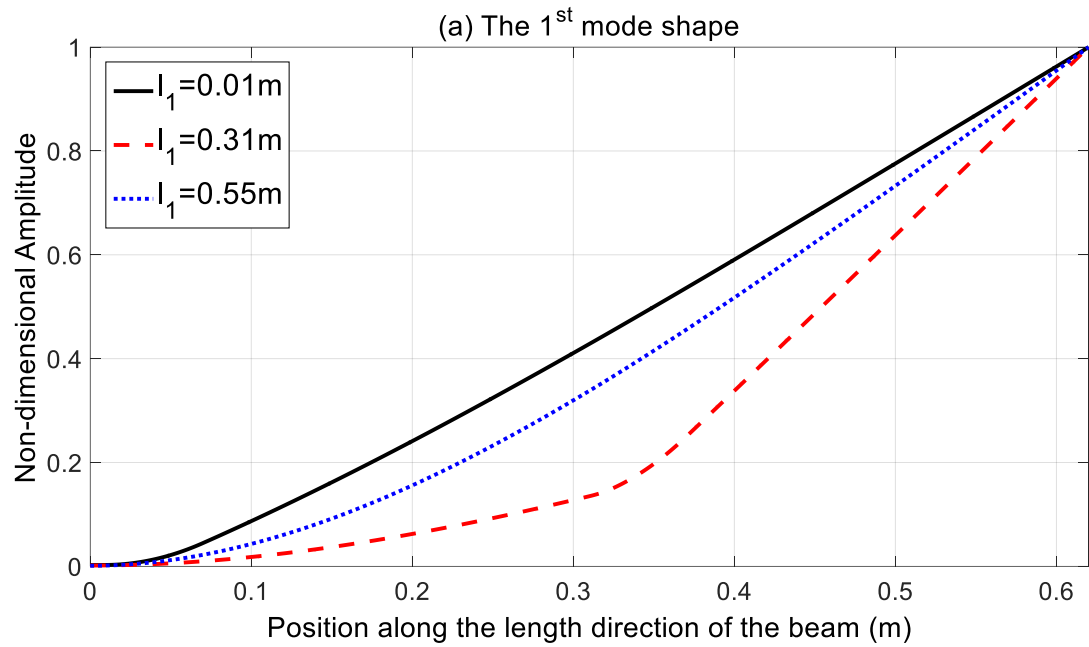


Fig. 4-5 Mode shapes of the cantilever beam with the activation of the piezoelectric actuator with different locations, where the values for $L_c=0.32$ m, $d=0.0012$ m and $g=8.5$.

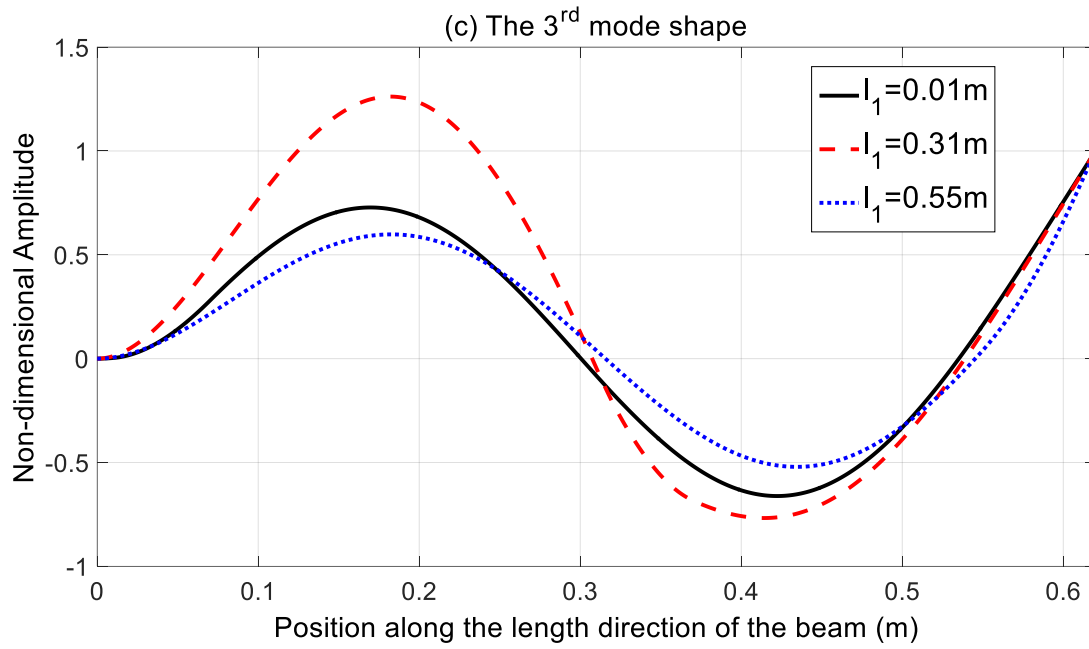


Fig. 4-5 Continued.

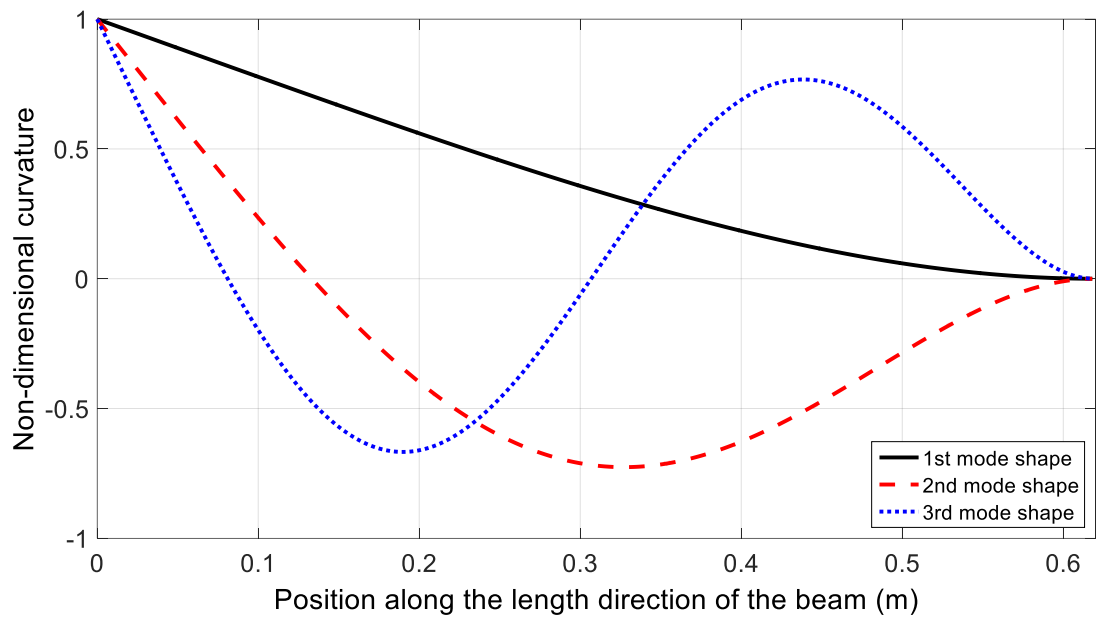


Fig. 4-6 The non-dimensional curvature distribution of the healthy cantilever beam without tuning.

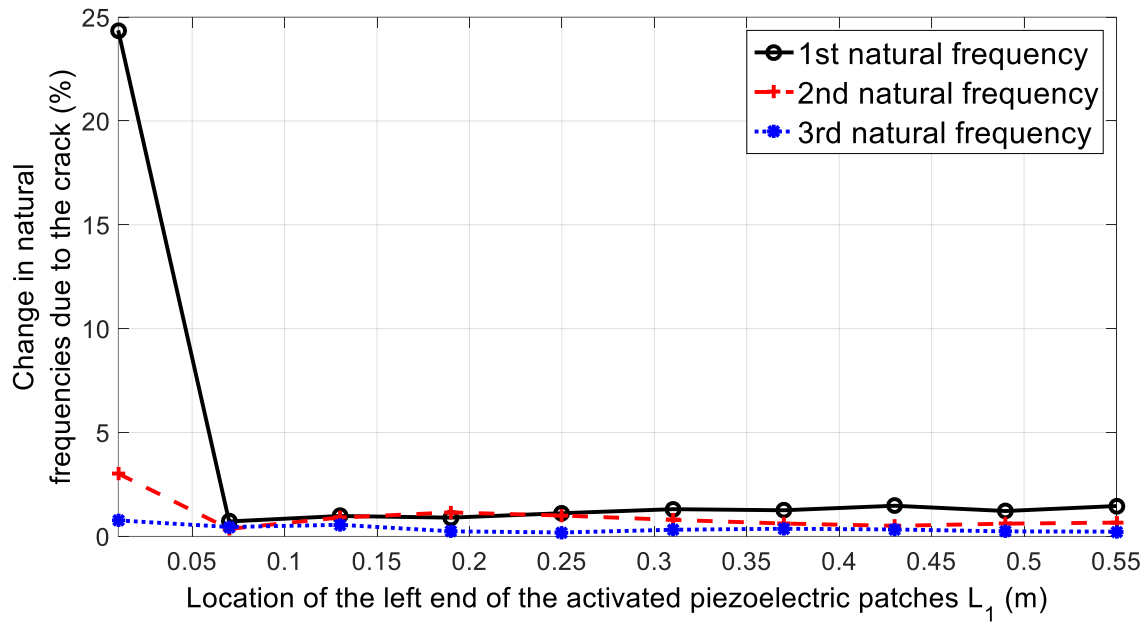


Fig. 4-7 The change in the natural frequencies of the cantilever beam due to the crack effect with different depth of the crack under the scan-tuning, where the values for $L_c=0.32$ m, $d=0.0012$, $g=8$.

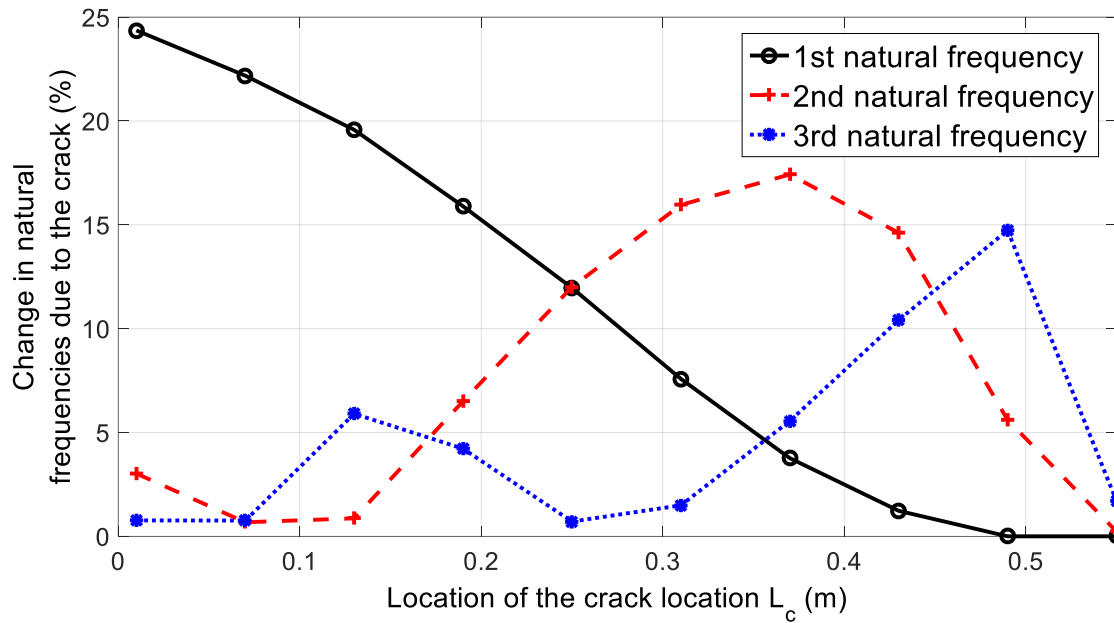


Fig. 4-8 The change in the natural frequencies of the cantilever beam due to the crack effect with different locations of the crack under the feedback excitation of the piezoelectric actuator that is close to the crack, where the values for $a=0.0012\text{m}$ and $g=8$.

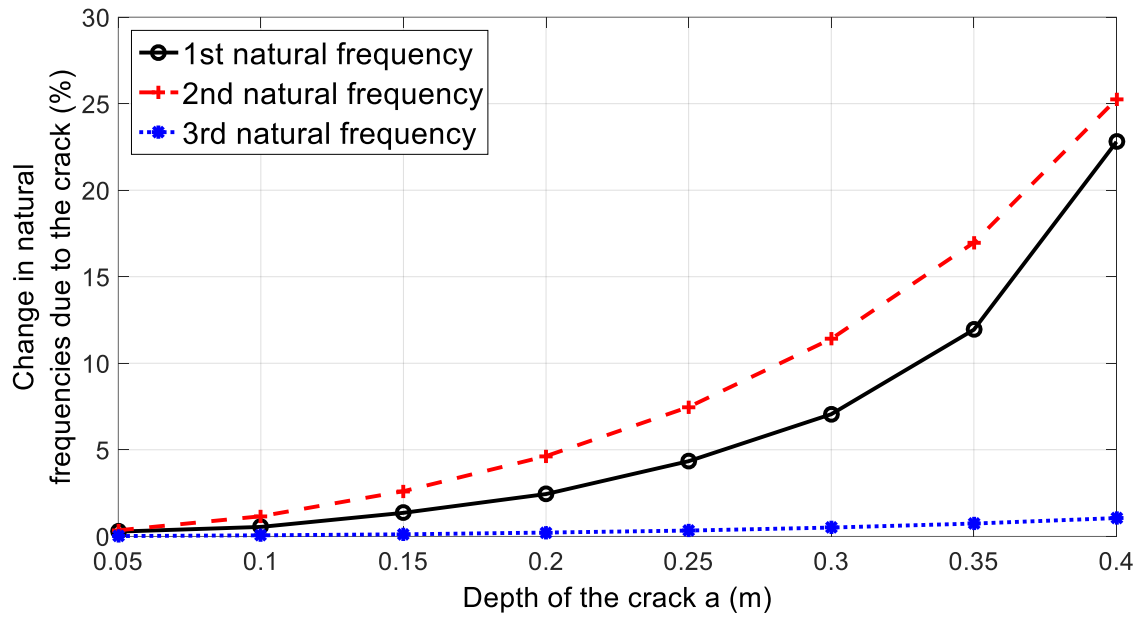


Fig. 4-9 The changes in the natural frequencies of the cantilever beam due to the crack with different depth under the scan-tuning with the fixed values of $L_c = 0.32$ m, $L_l = 0.31$ m, $g = 8.5$.

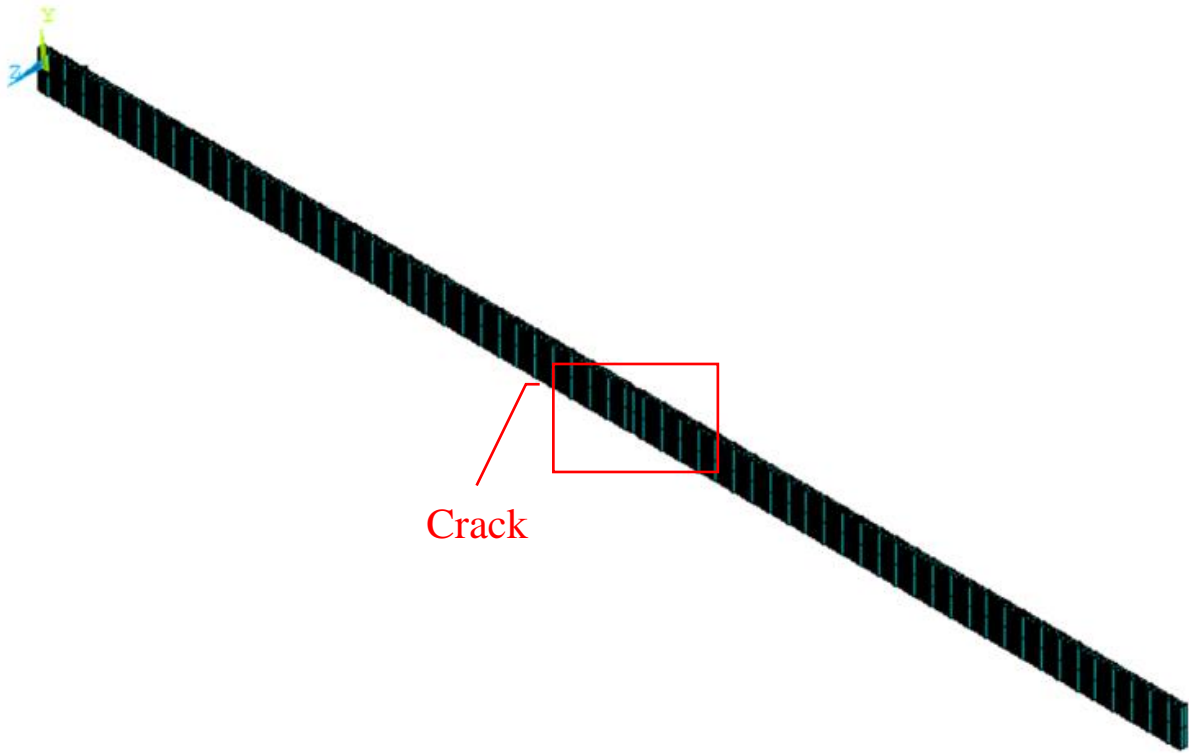
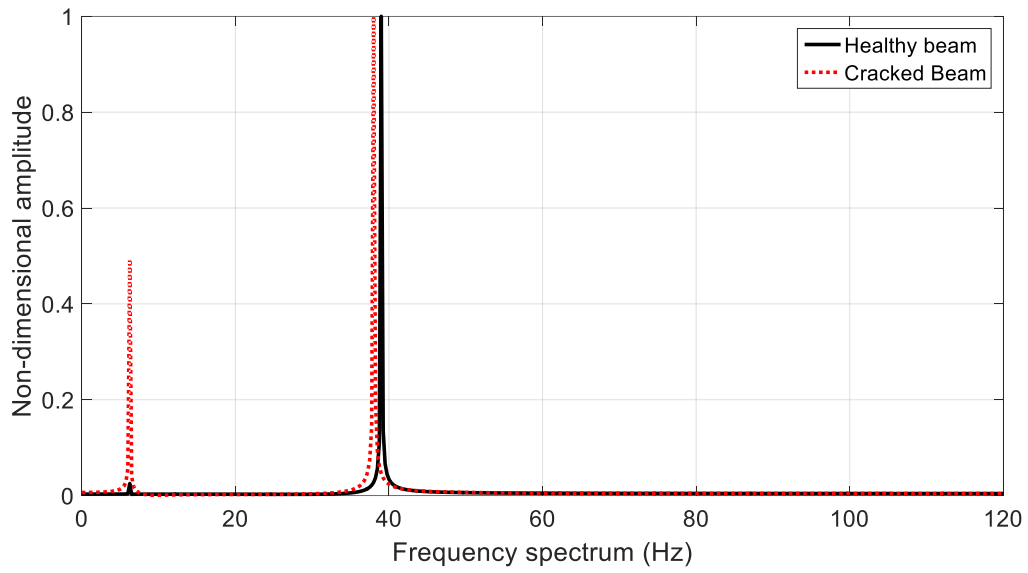
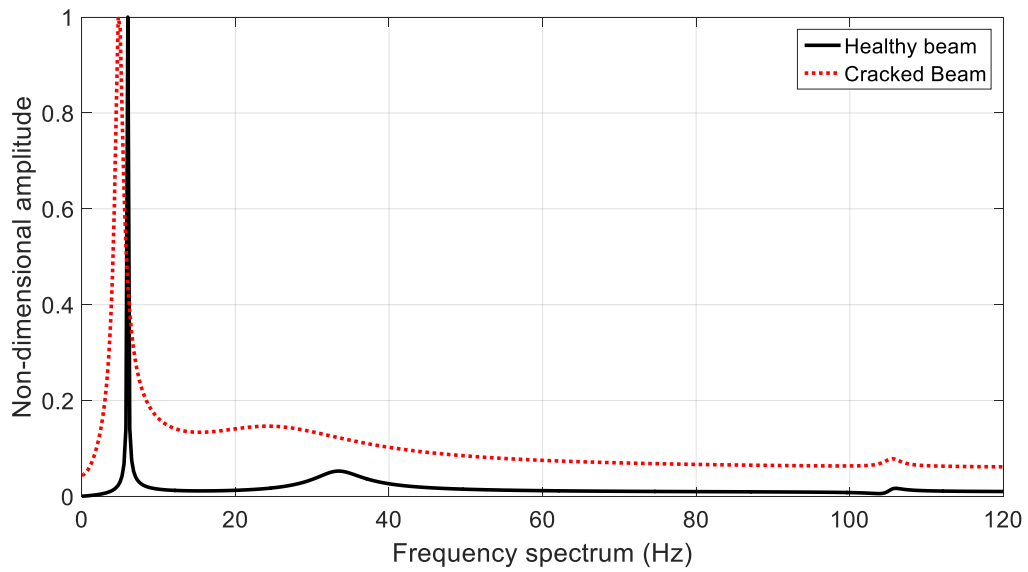


Fig. 4-10 Finite element model of a cantilever beam with a crack at $L_c=0.32\text{m}$



(a)



(b)

Fig. 4-11 Frequency spectrums of FEM simulations (a) without vibration tuning and (b) with vibration tuning at appropriate position

5. Delamination identification through a scan-tuning process using piezoelectric materials

In this chapter, the scan vibration tuning methodology coupled with piezoelectric materials is applied in delamination identification in beam-type structures. Similarly, the damage effect on the structure natural frequencies is magnified through the tuning process. Piezoelectric sensors and actuators on both surfaces of the host beam to generate the feedback bending excitations. Through the scan-tuning process by activating the piezoelectric actuator at different positions with decent gain, the delamination existence and location can be determined by the natural frequencies compared with the healthy beam.

5.1 Theoretical model

In this section, the overall flow of the scanning vibration tuning process in delamination identification is explained first. The first three natural frequencies of the tested structures are utilized to evaluate the delamination damage, including the determination of the existence, location and the size of the delamination. The theoretical models are subsequently proposed in details to calculate the damage effect on the natural frequencies.

Fig. 5-1 shows the physical model of a delaminated cantilever beam covered by piezoelectric patches. Following the same strategy in chapter 4, the expression of the dynamic equation of the piezoelectric coupled beam is can be expressed same as Eq. (4-1). To analyze the dynamic response of delaminated beam under the piezoelectric effect, the beam is supposed to be separated into certain number, N , of sections, according to the relative location between the activated piezoelectric patches and the delamination area. The vibration solutions of each section are listed as below:

$$\begin{aligned}
W_1(x) &= C_1 \cos \beta x + C_2 \sin \beta x + C_3 \cosh \beta x + C_4 \sinh \beta x, \\
W_2(x) &= C_5 \cos \beta x + C_6 \sin \beta x + C_7 \cosh \beta x + C_8 \sinh \beta x, \\
W_3(x) &= C_9 \cos \beta x + C_{10} \sin \beta x + C_{11} \cosh \beta x + C_{12} \sinh \beta x, \\
&\vdots \\
W_N(x) &= C_{4N-3} \cos \beta x + C_{4N-2} \sin \beta x + C_{4N-1} \cosh \beta x + C_{4N} \sinh \beta x,
\end{aligned} \tag{5-1}$$

where C_{1-N} are the unknown constants, β is real constant related with the natural frequency of the structure given by $\beta = \sqrt[4]{\omega^2 \frac{m'}{(EI)'}}$, and ω is the natural frequency of the beam. The expressions of m' and EI' are referred to Eq. (4-2).

Five cases regarding the relative location between the activated piezoelectric patches and the delamination area of the beam are considered. The length of the delamination is assumed to be greatly larger than the length of a single piezoelectric patch. The boundary and continuity conditions of each case are shown as Appendix C.

Substituting Eqs. (2-2), (2-13), (2-14) and (5-1) into boundary conditions and continuity conditions illustrated by Eqs. (C-1) to (C-5) and Figs. C-1 to C-5, the n th natural frequencies of the beam under the vibration tuning, $\omega'_{n,h}$ and $\omega'_{n,d}$ ($n=1, 2, 3, \dots, \infty$), can be solved by the Eigen value problem. By learning the delamination effect on the change of the natural frequencies compared to the healthy structure, the existence and size of the delamination can be determined. Detailed simulation results and discussions are presented in the next section.

5.2 Simulations and discussions

In this section, simulations based on the theoretical model are realized numerically. Two cases with different positions of the delamination in beam structure are considered, while one is located at the middle of the cantilever beam, and the other one is close to the fixed end. The percentage

change of the first three natural frequencies of both the healthy beam and the delaminated beam after scan-tuning are calculated. Effects of the size of the attached piezoelectric patches on delamination identification are also discussed. It is assumed that there is no gap between the two laminated section of the beam, and the required parameters for simulation are listed at Table 5-1.

Table 5-2 shows the results of the changes in natural frequencies of the beam without the scan vibration tuning process, with a delamination distributed at $0.22\text{m} < x < 0.32\text{m}$. The thickness of the beam is separated by the delamination into two sections with $h_{d1}=0.002\text{m}$ and $h_{d2}=0.001\text{m}$ respectively. It can be seen that the largest change in natural frequencies occurs in the 2nd natural frequency. The sensitivity with over 17% change of the 2nd natural frequency is high enough for the delamination detection. Another delamination with different size and location is also detected by the natural frequencies change as shown in Table 5-3. However, the location of the delamination distribution cannot be learned merely from the frequency change.

To enhance the sensitivity of the proposed method, proper gain of the amplifier is required. Previous study indicate that larger gain of the amplifier leads to more obvious change in the natural frequencies of the structure due to the damage. In consideration of the structural stability, when the delamination region ranges from $x=0.25\text{m}$ to $x=0.35\text{m}$, and the gain factor, g , is set as 6. The height of the upper and lower delaminated section of the beam is 0.002 m and 0.001 m respectively. Fig. 5-2 displays the detection results of the change in the first three beam natural frequencies due to the existence of the delamination with different size of the piezoelectric patches. From Fig. 5-2, it is found that the maximal percentage changes are 20%, 32% and 7% in the first three natural frequencies respectively, where $a = 0.06$. It is noted that with the vibration tuning, the delamination detection sensitivity with 32% change of the 2nd natural frequency of the beam due to the delamination is much higher than the case without vibration tuning (only 17% change of the 2nd

natural frequency). In addition, the damage effect on the 1st and the 2nd natural frequencies is much more significant than the 3rd one under scan vibration tuning. It is because the delamination induces stiffness reduction of the beam section and changes its curvature distribution as the crack does. However, little curvature is distributed on the middle section of the 3rd vibration mode shape, which leads to minor slope difference between both sides of the piezoelectric patches in the delamination region, as well as weak feedback excitation on the beam for damage detection. Overall, the existence of the middle delamination can be easily detected from frequency variation by the scan vibration tuning when $l_p = 0.06\text{m}$, but the location of the delamination cannot be accurately predicted. From Fig. 5-2, obvious damage effect on the natural frequencies is shown, when the fourth, fifth and sixth couple of piezoelectric patches are activated, pointing out that the delamination is roughly located within $0.19\text{m} < x < 0.37\text{m}$, which does not accurately match the exact delamination region ($0.22\text{m} < x < 0.32\text{m}$).

To better locate the delamination region, Figs. 5-2 and 5-3 display the detection results in natural frequencies change due to the delamination through scan vibration tuning to the same host beam, but the length of each discrete piezoelectric patches, l_p , is shorten into 0.03m and 0.01m respectively. The scan-tuning process with both sizes of the piezoelectric patches can detect the existence of the delamination with over 25% change in the 2nd natural frequency. Regarding the ability of delamination localization, as shown in Fig. 5-2 and 5-3, the delamination region is expected to lie within the range of $0.22\text{m} < x < 0.34\text{m}$ and $0.22\text{m} < x < 0.32\text{m}$ respectively. It is found that with shorter length of the piezoelectric patches, the delamination region is supposed to be more accurately located.

To further illustrate the effectiveness of the scan vibration tuning, another cantilever beam with different delamination region is also studied. The delamination region is close to the fixed end,

initiating at $x=0.10\text{m}$ and ends at $x=0.15\text{m}$. Unlike the detection results for the delamination located at the middle section of the beam, as shown in Fig. 5-4, the 1st natural frequency shows the highest sensitivity, up to 21.45% change, of the detection on the delamination around the fixed end of the beam. The 3rd natural frequency comes the second with 8.86% change. Both the 1st and the 3rd natural frequencies are able to predict the delamination location correctly. On the contrary, the delamination effect on the 2nd natural frequency is extremely weak, with less than 1% change. This phenomenon is also attributed to the limited curvature distribution at the delamination region in the specific mode shape of the beam.

5.3 Summary

A scan vibration tuning process by the use of piezoelectric materials is applied to detect and locate the delamination inside the beam-type structures. The piezoelectric sensor patches and actuator patches are attached in pairs on both sides of the beams to generate the feedback excitations and magnify the delamination effect on structure natural frequencies changes. The scan vibration tuning process is realized by the activation of each pair of piezoelectric patches individually with a feedback tuning process throughout the beam. The natural frequency change compared with the healthy beam also under scan vibration tuning is then studied from the free vibration response. From the numerical simulations, delamination at the center or around the fixed end of the beam can be detected with over 20% shift in specific natural frequencies. Optimal design of the size of the piezoelectric patches is also studied to reach more accurate locating of the delamination. Overall, the proposed methodology is effective on beam delamination identification from the theoretical study with great potential for the application on other types of structures as well.

Table 5-1 Geometric and material properties for numerical simulations

Parameter	Host beam (aluminum)	Piezoelectric patches
Young's modulus (N m ⁻²)	$E=69\times 10^9$	$E_p=78\times 10^9$
Mass density (kg m ⁻³)	$\rho=2.8\times 10^3$	$\rho_p=7.5\times 10^3$
e_{31} (C m ⁻²)	-	-2.8
d_{31} (C N ⁻¹)	-	-1.28×10^{-10}
C_v (nF)	-	0.643 for a piezoelectric patch with dimensions of 0.01m×0.06m×0.00035m
L (m)	0.62	-
L_1 (m)	0.01, 0.02, ..., 0.60 ($l_p=0.01$) 0.01, 0.04, ..., 0.58 ($l_p=0.03$) 0.01, 0.07, ..., 0.55 ($l_p=0.06$)	-
L_2 (m)	$L_1 + l_p$	-
L_{d1} (m)	0.10, 0.22	-
L_{d2} (m)	0.15, 0.32	-
h (m)	0.003	-
h_1 (m)	-	0.00035
h_{d1} (m)	0.002	-
h_{d2} (m)	0.001	-
b (m)	0.02	-
b_s (m)	-	0.01
b_a (m)	-	0.01
l_p (m)	-	0.01, 0.03, 0.06

Table 5-2 Difference in natural frequencies for healthy and delaminated beams without vibration tuning ($L_{d1}=0.22\text{m}$, $L_{d2}=0.32\text{m}$)

	1st order	2nd order	3rd order
Healthy beam (Hz)	6.41	40.25	112.70
Delaminated beam (Hz)	5.78	33.31	105.98
Percentage of variation	9.93	17.24	5.96
(%)			

Table 5-3 Difference in natural frequencies for healthy and delaminated beams without vibration tuning ($L_{d1}=0.10\text{m}$, $L_{d2}=0.15\text{m}$)

	1st order	2nd order	3rd order
Healthy beam (Hz)	6.41	40.25	112.70
Delaminated beam (Hz)	5.52	40.09	107.67
Percentage of variation	13.90	0.34	4.47
(%)			

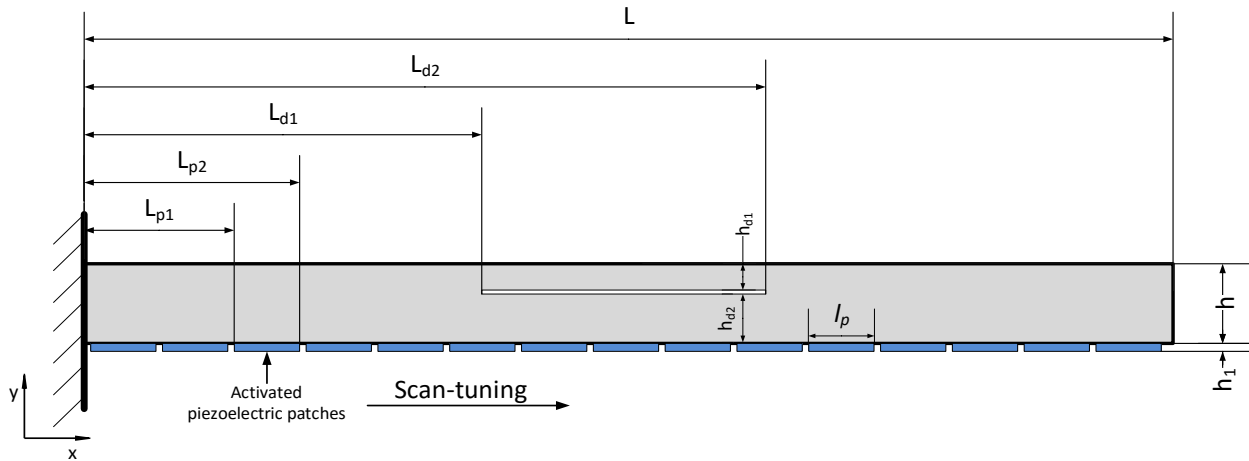


Fig. 5-1 Physical model of a delaminated cantilever beam coupled with piezoelectric patches

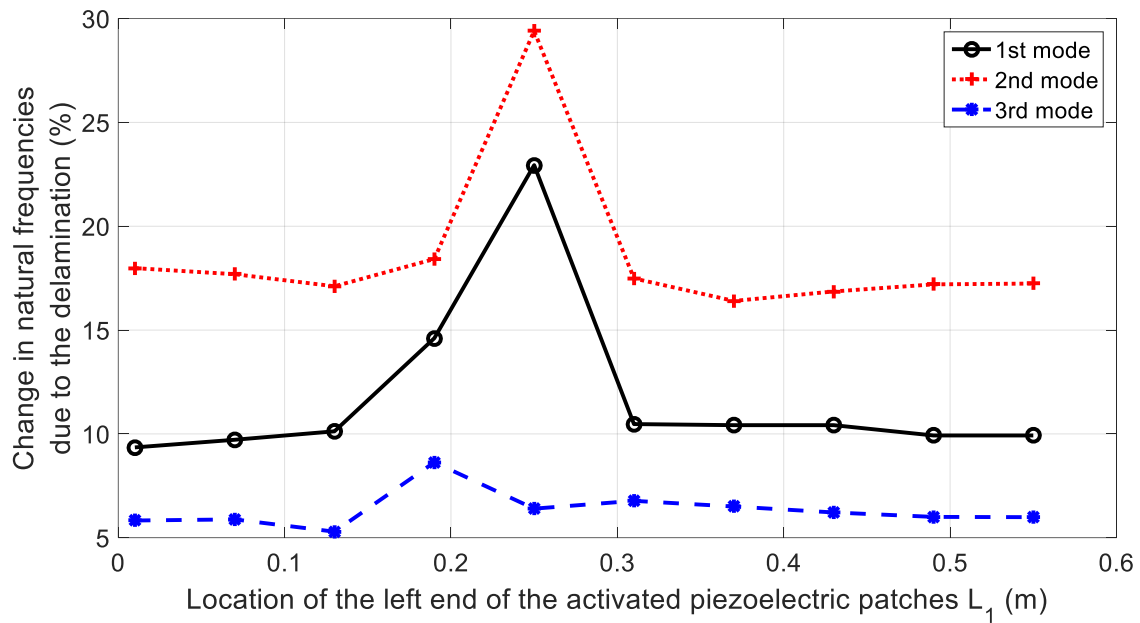


Fig. 5-2 The change in the natural frequencies of the cantilever beam due to the delamination effect under the scan-tuning, where the values for $L_{d1}=0.22\text{m}$, $L_{d2}=0.32\text{m}$, $l_p=0.06\text{m}$ and $g=6$.

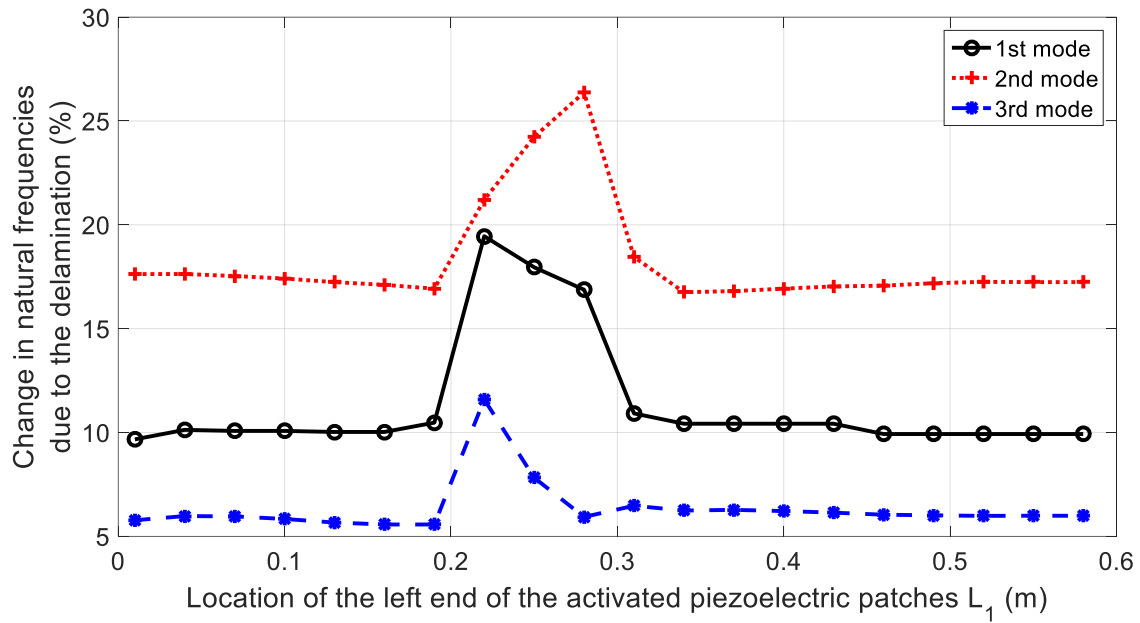


Fig. 5-3 The change in the natural frequencies of the cantilever beam due to the delamination effect under the scan-tuning, where the values for for $L_{d1}=0.22\text{m}$, $L_{d2}=0.32\text{m}$, $l_p=0.03\text{m}$ and $g=6$.

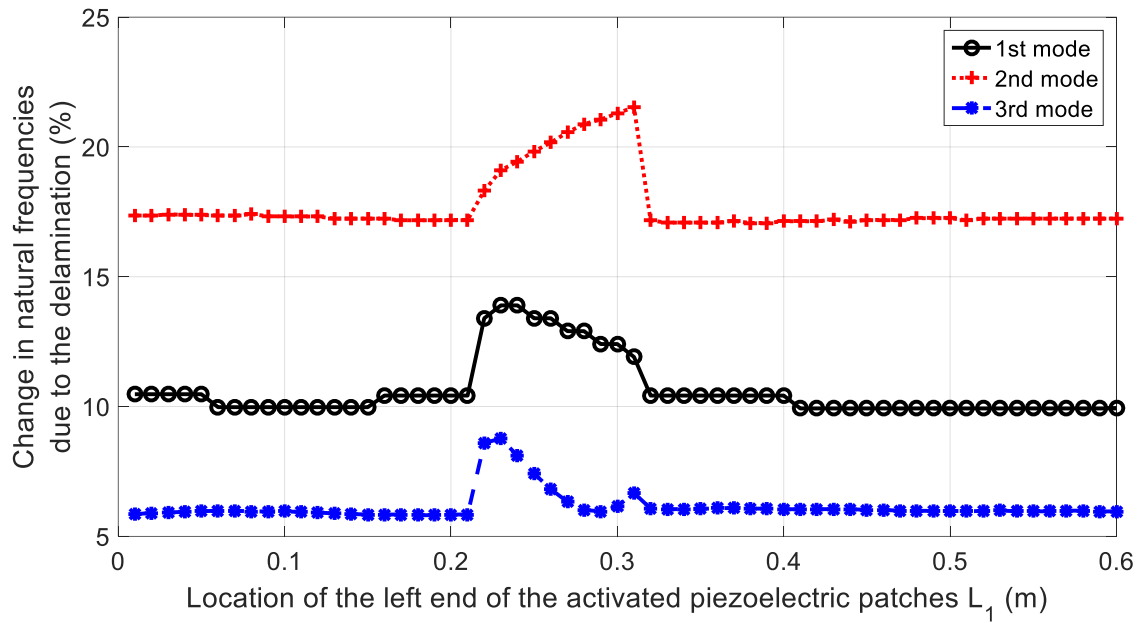


Fig. 5-4 The change in the natural frequencies of the cantilever beam due to the delamination effect under the scan-tuning, where the values for $L_{d1}=0.22\text{m}$, $L_{d2}=0.32\text{m}$, $l_p=0.01\text{m}$ and $g=6$.

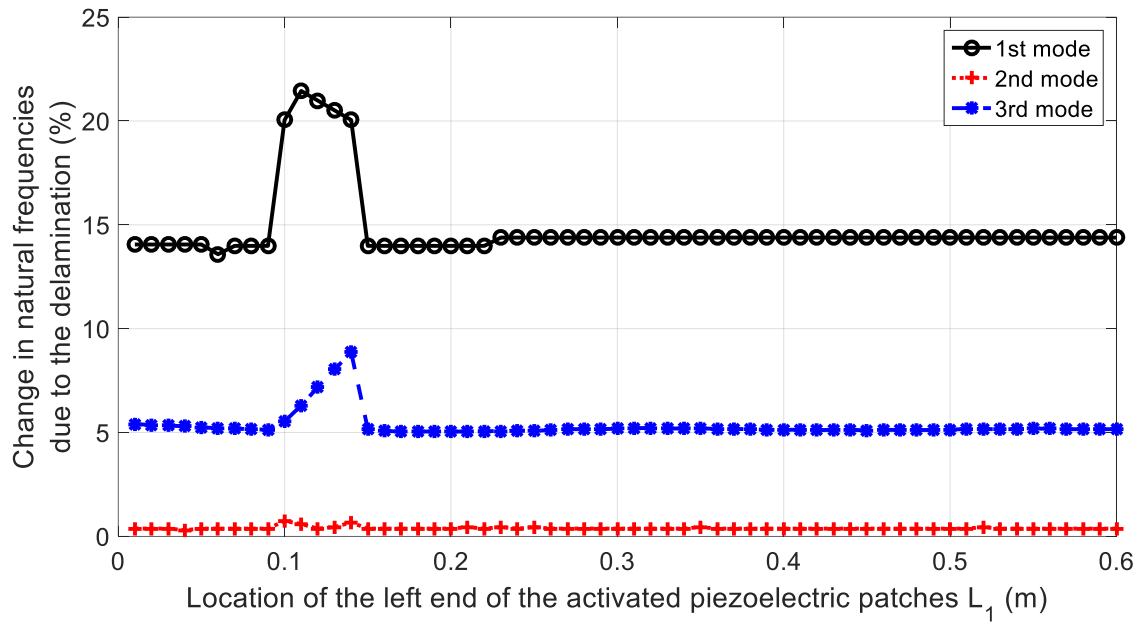


Fig. 5-5 The change in the natural frequencies of the cantilever beam due to the delamination effect under the scan-tuning, where the values for $L_{d1}=0.10\text{m}$, $L_{d2}=0.15\text{m}$, $l_p=0.01\text{m}$ and $g=6$.

6. Conclusions and future works

In this thesis, focusing on natural frequency based methods, the development of vibration based damage detection is reviewed first. The review of the applications of piezoelectric materials in damage identification is followed. It is found that the natural frequencies of the structure may be easily extracted from the vibration response, but they are insensitive to damage occurrence. To improve the sensitivity of damage detection, an optimally designed vibration characteristic tuning technique coupled with piezoelectric materials is proposed. The feedback bending moments induced by the piezoelectric sensors and actuators are utilized to tune the vibration characteristics of the structure including the vibration mode shapes and natural frequencies. The damage effect on the change of natural frequencies is hence significantly enhanced for damage detection. Following the proposed technique, a scan-tuning methodology is developed for damage detection and localization in beam-type structures. Different types of damages (crack and delamination) in beams are studied numerically to reveal the universality of the methodology.

The main contribution of this research is to propose alternative natural frequency based methods for damage identification on engineering structures. By the use of piezoelectric materials, an advanced vibration characteristic tuning technique is developed to diminish the environment effect so as to increase the sensitivity of the damage detection. From the numerical simulations (both analytical and FEM), following findings and conclusions can be made.

- I. A detailed theoretical model is provided to reveal the principle of the vibration characteristic tuning process by piezoelectric materials.

- II. High sensitivity for crack detection is realized via the proposed technique. From the analytical simulations, the change in the 1st natural frequency due to the fix-end crack existence in a cantilever beam is found to increase from 3.3% to 18 % under the tuning process.
- III. The optimal design of the size and placement of the piezoelectric layers is conducted to achieve higher sensitivity for damage detection.
- IV. As an extended study of the proposed technique, the scan-tuning methodology is designed to not only detect but also locate the damage in beams based on the natural frequency shift. With over 20% change in the natural frequencies, both the crack and delamination damages in beams are efficiently detected and located through the scan-tuning process.
- V. Parameter study of the crack depth and the amplifier gain is demonstrated to optimize the scan-tuning process.
- VI. A finite element model is constructed to verify the effectiveness of the scan-tuning methodology for crack detection and localization.
- VII. The length of the piezoelectric patches for scan-tuning is optimally designed to estimate the more accurate location of the damage.

Overall, the detection and localization of damages in beam-type structures (e.g. crack and delamination) are realized by utilizing the piezoelectric materials depending on numerical simulations.

The research work is still on the preliminary stage. Major future research is to conduct a series of experiments to verify the feasibility of the proposed techniques and methods. The selection of the voltage amplifier is critical since the signal from the piezoelectric sensor is extremely susceptible to the noise. In addition, the Level 3 of SHM, which is the quantification of the severity of the

damage, will be further studied through the proposed technique. Lastly, the potential of the proposed methods for damage identification to other types of structures, such as plates and frames, is also noted. Further studies on different structures are required to build up a complete damage monitoring system.

Reference

- [1] A. Rytter, Vibrational based inspection of civil engineering structures, (1993).
- [2] E.P. Carden, P. Fanning, Vibration based condition monitoring: a review, Structural health monitoring, 3 (2004) 355-377.
- [3] J.-J. Sinou, A review of damage detection and health monitoring of mechanical systems from changes in the measurement of linear and non-linear vibrations, Mechanical Vibrations: Measurement, Effects and Control, (2009) 643-702.
- [4] O. Salawu, Detection of structural damage through changes in frequency: a review, Engineering structures, 19 (1997) 718-723.
- [5] K.R. Kumar, S. Narayanan, Active vibration control of beams with optimal placement of piezoelectric sensor/actuator pairs, Smart Materials and Structures, 17 (2008) 055008.
- [6] N. Wu, Q. Wang, An experimental study on the repair of a notched beam subjected to dynamic loading with piezoelectric patches, Smart Materials and Structures, 20 (2011) 115023.
- [7] Q. Wang, S. Quek, K. Liew, On the repair of a cracked beam with a piezoelectric patch, Smart materials and structures, 11 (2002) 404.
- [8] L. RAY, L. TIAN, Damage Detection in Smart Structures Through Sensitivity Enhancing Feedback Control, Journal of Sound Vibration, 227 (1999) 987-1002.
- [9] N. Wu, Modeling and Application of Piezoelectric Materials in Repair of Engineering Structures, (2012).
- [10] Y.-S. Lee, M.-J. Chung, A study on crack detection using eigenfrequency test data, Computers & structures, 77 (2000) 327-342.
- [11] S. Chinchalkar, Determination of crack location in beams using natural frequencies, Journal of Sound and vibration, 247 (2001) 417-429.

- [12] O.S. Salawu, C. Williams, Bridge assessment using forced-vibration testing, *Journal of structural engineering*, 121 (1995) 161-173.
- [13] S. Alampalli, G. Fu, E.W. Dillon, Signal versus noise in damage detection by experimental modal analysis, *Journal of Structural Engineering*, 123 (1997) 237-245.
- [14] A.A. Elshafey, H. Marzouk, M. Haddara, Experimental damage identification using modified mode shape difference, *Journal of Marine Science and Application*, 10 (2011) 150-155.
- [15] G. Yan, X. Peng, H. Hao, Localization of free-spanning damage using mode shape curvature, in: *Journal of Physics: Conference Series*, IOP Publishing, 2011, pp. 012017.
- [16] D.J. Ewins, *Modal testing: theory and practice*, Research studies press Letchworth, 1984.
- [17] N.M.M. Maia, J.M.M. e Silva, *Theoretical and experimental modal analysis*, Research Studies Press, 1997.
- [18] P.F. Pai, L.G. Young, Damage detection of beams using operational deflection shapes, *International journal of solids and structures*, 38 (2001) 3161-3192.
- [19] K. Waldron, A. Ghoshal, M. Schulz, M. Sundaresan, F. Ferguson, P. Pai, J. Chung, Damage detection using finite element and laser operational deflection shapes, *Finite Elements in Analysis and Design*, 38 (2002) 193-226.
- [20] E. Asnaashari, J.K. Sinha, Development of residual operational deflection shape for crack detection in structures, *Mechanical Systems and Signal Processing*, 43 (2014) 113-123.
- [21] R. Sampaio, N. Maia, R. Almeida, A. Urgueira, A simple damage detection indicator using operational deflection shapes, *Mechanical Systems and Signal Processing*, 72 (2016) 629-641.
- [22] W. Fan, P. Qiao, Vibration-based damage identification methods: a review and comparative study, *Structural Health Monitoring*, 10 (2011) 83-111.

- [23] J.-T. Kim, N. Stubbs, Model-uncertainty impact and damage-detection accuracy in plate girder, *Journal of Structural Engineering*, 121 (1995) 1409-1417.
- [24] Z. Shi, S. Law, L.M. Zhang, Structural damage detection from modal strain energy change, *Journal of engineering mechanics*, 126 (2000) 1216-1223.
- [25] W.-J. Yan, T.-L. Huang, W.-X. Ren, Damage detection method based on element modal strain energy sensitivity, *Advances in Structural Engineering*, 13 (2010) 1075-1088.
- [26] C.R. Farrar, S.W. Doebling, D.A. Nix, Vibration-based structural damage identification, *Philosophical Transactions of the Royal Society of London A: Mathematical, Physical and Engineering Sciences*, 359 (2001) 131-149.
- [27] A. Messina, E. Williams, T. Contursi, Structural damage detection by a sensitivity and statistical-based method, *Journal of sound and vibration*, 216 (1998) 791-808.
- [28] P. Fanning, E. Carden, Auto-regression and statistical process control techniques applied to damage indication in telecommunication masts, in: *Key Engineering Materials*, Trans Tech Publ, 2001, pp. 251-260.
- [29] W.-J. Yan, W.-X. Ren, T.-L. Huang, Statistic structural damage detection based on the closed-form of element modal strain energy sensitivity, *Mechanical Systems and Signal Processing*, 28 (2012) 183-194.
- [30] K. Worden, G. Manson, N. Fieller, Damage detection using outlier analysis, *Journal of Sound and Vibration*, 229 (2000) 647-667.
- [31] P. Cawley, R. Adams, The location of defects in structures from measurements of natural frequencies, *The Journal of Strain Analysis for Engineering Design*, 14 (1979) 49-57.
- [32] R.Y. Liang, F.K. Choy, J. Hu, Detection of cracks in beam structures using measurements of natural frequencies, *Journal of the Franklin Institute*, 328 (1991) 505-518.

- [33] H. Banks, D. Inman, D. Leo, Y. Wang, An experimentally validated damage detection theory in smart structures, *Journal of Sound and Vibration*, 191 (1996) 859-880.
- [34] B. Morgan, R. Oesterle, On-site modal analysis-a new powerful inspection technique, in: *Proceedings of the 2nd International Bridge Conference*, Pittsburg, Pennsylvania, 1985, pp. 108-114.
- [35] S. Zhong, S.O. Oyadiji, K. Ding, Response-only method for damage detection of beam-like structures using high accuracy frequencies with auxiliary mass spatial probing, *Journal of Sound and Vibration*, 311 (2008) 1075-1099.
- [36] H. Wang, Study on natural-frequency-based structural damage identification of steel transmission tower, in: *Transportation, Mechanical, and Electrical Engineering (TMEE), 2011 International Conference on*, IEEE, 2011, pp. 1382-1385.
- [37] S.-Q. Wang, H.-J. Li, Assessment of structural damage using natural frequency changes, *Acta Mechanica Sinica*, 28 (2012) 118-127.
- [38] S.-H. Chao, C.-H. Loh, M.-H. Tseng, Structural damage assessment using output-only measurement: Localization and quantification, *Journal of Intelligent Material Systems and Structures*, 25 (2014) 1097-1106.
- [39] I. Negru, G. Gillich, Z. Praisach, M. Tufoi, N. Gillich, Natural frequency changes due to damage in composite beams, in: *Journal of Physics: Conference Series*, IOP Publishing, 2015, pp. 012091.
- [40] Y. Zou, L. Tong, G. Steven, Vibration-based model-dependent damage (delamination) identification and health monitoring for composite structures—a review, *Journal of Sound and vibration*, 230 (2000) 357-378.

- [41] Q. Wang, W. Duan, S.T. Quek, Repair of notched beam under dynamic load using piezoelectric patch, *International journal of mechanical sciences*, 46 (2004) 1517-1533.
- [42] N. Wu, Q. Wang, Repair of vibrating delaminated beam structures using piezoelectric patches, *Smart Materials and Structures*, 19 (2010) 035027.
- [43] A.S. Islam, K.C. Craig, Damage detection in composite structures using piezoelectric materials (and neural net), *Smart Materials and Structures*, 3 (1994) 318.
- [44] A.C. Okafor, K. Chandrashekhara, Y. Jiang, Delamination prediction in composite beams with built-in piezoelectric devices using modal analysis and neural network, *Smart materials and structures*, 5 (1996) 338.
- [45] C.H. Keilers, F.-K. Chang, Identifying delamination in composite beams using built-in piezoelectrics: part I—experiments and analysis, *Journal of Intelligent Material Systems and Structures*, 6 (1995) 649-663.
- [46] C.H. Keilers, F.-K. Chang, Identifying Delamination in Composite Beams Using Built-In Piezoelectrics Part II—An Identification Method, *Journal of Intelligent Material Systems and Structures*, 6 (1995) 664-672.
- [47] X. Jian, H. Tzou, C. Lissenden, L. Penn, Damage detection by piezoelectric patches in a free vibration method, *Journal of composite materials*, 31 (1997) 345-359.
- [48] C.P. De Vera, J. Guemes, Embedded self-sensing piezoelectric for damage detection, *Structural Health Monitoring: Current Status and Perspectives*, 445 (1998).
- [49] Z. Su, L. Ye, X. Bu, A damage identification technique for CF/EP composite laminates using distributed piezoelectric transducers, *Composite structures*, 57 (2002) 465-471.
- [50] X. Liu, Z. Jiang, L. Ji, Investigation on the design of piezoelectric actuator/sensor for damage detection in beam with Lamb waves, *Experimental Mechanics*, 53 (2013) 485-492.

- [51] E. Hadjigeorgiou, G. Stavroulakis, C. Massalas, Shape control and damage identification of beams using piezoelectric actuation and genetic optimization, *International Journal of Engineering Science*, 44 (2006) 409-421.
- [52] L. Jiang, J. Tang, K. Wang, An enhanced frequency-shift-based damage identification method using tunable piezoelectric transducer circuitry, *Smart Materials and Structures*, 15 (2006) 799.
- [53] L. Jiang, J. Tang, K. Wang, On the tuning of variable piezoelectric transducer circuitry network for structural damage identification, *Journal of Sound and Vibration*, 309 (2008) 695-717.
- [54] J. Zhao, J. Tang, K. Wang, Enhanced statistical damage identification using frequency-shift information with tunable piezoelectric transducer circuitry, *Smart Materials and Structures*, 17 (2008) 065003.
- [55] Y. Yang, H. Liu, V.G.M. Annamdas, Parallel and individual interrogations of piezo-impedance transducers for damage detection, *Materials and Manufacturing Processes*, 25 (2010) 249-254.
- [56] S. Bhalla, R. Panigrahi, A. Gupta, Damage assessment of tensegrity structures using piezo transducers, *Meccanica*, 48 (2013) 1465-1478.
- [57] C. Providakis, G. Angeli, M. Favvata, N. Papadopoulos, C. Chalioris, C. Karayannis, Detection of concrete reinforcement damage using piezoelectric materials-Analytical and experimental Study, *International Journal of Civil, Architectural, Structural and Construction Engineering*, 8 (2014) 197-205.
- [58] C.-K. Lee, F.C. Moon, Modal sensors/actuators, *Journal of applied mechanics*, 57 (1990) 434-441.
- [59] C.-C. Lin, C.-Y. Hsu, Static shape control of smart beam plates laminated with piezo sensors and actuators, *Smart materials and structures*, 8 (1999) 519.

- [60] E.F. Crawley, J. De Luis, Use of piezoelectric actuators as elements of intelligent structures, AIAA journal, 25 (1987) 1373-1385.
- [61] M. Krawczuk, W. Ostachowicz, Modelling and vibration analysis of a cantilever composite beam with a transverse open crack, Journal of Sound and Vibration, 183 (1995) 69-89.
- [62] Q. Wang, S. Quek, Enhancing flutter and buckling capacity of column by piezoelectric layers, International journal of solids and structures, 39 (2002) 4167-4180.
- [63] S. Zhao, N. Wu, Y. Cheng, High Sensitivity Damage Detection With Vibration Mode Shape Tuning Through the Optimal Design of Piezoelectric Actuators, in: ASME 2015 International Mechanical Engineering Congress and Exposition, American Society of Mechanical Engineers, 2015, pp. V04BT04A038-V004BT004A038.
- [64] S. Zhao, N. Wu, Q. Wang, Damage Detection of Beams by a Vibration Characteristic Tuning Technique Through an Optimal Design of Piezoelectric Layers, International Journal of Structural Stability and Dynamics, (2015) 1550070.
- [65] A.N.S. Institute, F. IEEE Ultrasonics, F.C.S.S. Committee, I.o. Electrical, E. Engineers, IEEE Standard on Piezoelectricity, IEEE, 1988.

Appendix A Linear piezoelectric constitutive equations (LPCE)

The standard form of the piezoelectric constitutive equations [65] can be written in four different forms as:

Strain-Charge form:

$$S_{ij} = s_{ijkl}^E T_{kl} + d_{kij} E_k \quad (\text{A-1})$$

$$D_i = d_{ikl} T_{kl} + \epsilon_{ik}^D E_k \quad (\text{A-2})$$

Strain-Voltage form:

$$S_{ij} = s_{ijkl}^D T_{kl} + g_{kij} D_k \quad (\text{A-3})$$

$$E_i = -g_{ikl} T_{kl} + \beta_{ik}^T D_k \quad (\text{A-4})$$

Stress-Voltage form:

$$T_{ij} = c_{ijkl}^D S_{kl} - h_{kij} D_k \quad (\text{A-5})$$

$$E_i = -h_{ikl} S_{kl} + \beta_{ik}^S D_k \quad (\text{A-6})$$

Stress-Charge form:

$$T_{ij} = c_{ijkl}^E S_{kl} - e_{kij} E_k \quad (\text{A-7})$$

$$D_i = e_{ikl} S_{kl} + \epsilon_{ij}^S E_k \quad (\text{A-8})$$

where the meanings and units of the symbols are listed in Table A-1.

Table A-1 List of symbols and their units

Symbol	Units	Physical Meaning
T_{ij}	$\frac{N}{m^2}$	stress components
S_{ij}	$\frac{m}{m}$	strain components
E_i	$\frac{N}{C}$	electric field components
D_i	$\frac{C}{m^2}$	electric charge density displacement components
s_{ijkl}^E	$\frac{m^2}{N}$	compliance coefficients
c_{ijkl}^E	$\frac{N}{m^2}$	stiffness coefficients
ϵ_{ij}^S	$\frac{F}{m}$	electric permittivity
d_{kij}	$\frac{C}{N}$	piezoelectric coupling coefficients for Strain-Charge form
e_{ikl}	$\frac{C}{m^2}$	piezoelectric coupling coefficients for Stress-Charge form
g_{ikl}	$\frac{m^2}{C}$	piezoelectric coupling coefficients for Strain-Voltage form
h_{ikl}	$\frac{N}{C}$	piezoelectric coupling coefficients for Stress-Voltage form

Appendix B Boundary and continuity conditions of beams under scan vibration tuning for crack identification

I. Boundary and continuity conditions of crack beams if $L_2 < L_c$:

$$\begin{aligned}
 x = 0 : w_1 = 0, \quad \frac{\partial w_1}{\partial x} = 0 ; \\
 x = L_1 : w_1 = w_2, \quad \frac{\partial w_1}{\partial x} = \frac{\partial w_2}{\partial x}, \\
 (EI)' \frac{\partial^2 w_1}{\partial x^2} - M_e = (EI)' \frac{\partial^2 w_2}{\partial x^2}, \quad (EI)' \frac{\partial^3 w_1}{\partial x^3} = (EI)' \frac{\partial^3 w_2}{\partial x^3}; \\
 x = L_2 : w_2 = w_3, \quad \frac{\partial w_2}{\partial x} = \frac{\partial w_3}{\partial x}, \\
 (EI)' \frac{\partial^2 w_2}{\partial x^2} = (EI)' \frac{\partial^2 w_3}{\partial x^2} - M_e, \quad (EI)' \frac{\partial^3 w_2}{\partial x^3} = (EI)' \frac{\partial^3 w_3}{\partial x^3}; \\
 x = L_c : w_3 = w_4, \quad \frac{\partial w_3}{\partial x} + \theta = \frac{\partial w_4}{\partial x} \text{ (With crack)}; \quad \frac{\partial w_3}{\partial x} = \frac{\partial w_4}{\partial x} \text{ (Without crack)}, \\
 (EI)' \frac{\partial^2 w_3}{\partial x^2} = (EI)' \frac{\partial^2 w_4}{\partial x^2}, \quad (EI)' \frac{\partial^3 w_3}{\partial x^3} = (EI)' \frac{\partial^3 w_4}{\partial x^3}; \\
 x = L : \frac{\partial^2 w_4}{\partial x^2} = 0, \quad \frac{\partial^3 w_4}{\partial x^3} = 0.
 \end{aligned} \tag{B-1}$$

II. Boundary and continuity conditions of crack beams if $L_1 \leq L_c$ and $L_2 \geq L_c$:

$$\begin{aligned}
x = 0 : w_1 = 0, \quad \frac{\partial w_1}{\partial x} = 0 ; \\
x = L_1 : w_1 = w_2, \quad \frac{\partial w_1}{\partial x} = \frac{\partial w_2}{\partial x}, \\
(EI)' \frac{\partial^2 w_1}{\partial x^2} - M_e = (EI)' \frac{\partial^2 w_2}{\partial x^2}, \quad (EI)' \frac{\partial^3 w_1}{\partial x^3} = (EI)' \frac{\partial^3 w_2}{\partial x^3}; \\
x = L_c : w_2 = w_3, \quad \frac{\partial w_2}{\partial x} + \theta = \frac{\partial w_3}{\partial x} \text{ (With crack)}; \quad \frac{\partial w_2}{\partial x} = \frac{\partial w_3}{\partial x} \text{ (Without crack)}, \\
(EI)' \frac{\partial^2 w_2}{\partial x^2} = (EI)' \frac{\partial^2 w_3}{\partial x^2}, \quad (EI)' \frac{\partial^3 w_2}{\partial x^3} = (EI)' \frac{\partial^3 w_3}{\partial x^3}; \\
x = L_2 : w_3 = w_4, \quad \frac{\partial w_3}{\partial x} = \frac{\partial w_4}{\partial x}, \\
(EI)' \frac{\partial^2 w_3}{\partial x^2} = (EI)' \frac{\partial^2 w_4}{\partial x^2} - M_e, \quad (EI)' \frac{\partial^3 w_3}{\partial x^3} = (EI)' \frac{\partial^3 w_4}{\partial x^3}; \\
x = L : \frac{\partial^2 w_4}{\partial x^2} = 0, \quad \frac{\partial^3 w_4}{\partial x^3} = 0.
\end{aligned} \tag{B-2}$$

III. Boundary and continuity conditions of crack beams if $L_1 > L_c$:

$$\begin{aligned}
 x = 0 : w_1 = 0, \quad \frac{\partial w_1}{\partial x} = 0; \\
 x = L_c : w_1 = w_2, \quad \frac{\partial w_1}{\partial x} + \theta = \frac{\partial w_2}{\partial x} \quad (\text{With crack}), \quad \frac{\partial w_1}{\partial x} = \frac{\partial w_2}{\partial x} \quad (\text{Without crack}), \\
 (EI)' \frac{\partial^2 w_1}{\partial x^2} = (EI)' \frac{\partial^2 w_2}{\partial x^2}, \quad (EI)' \frac{\partial^3 w_1}{\partial x^3} = (EI)' \frac{\partial^3 w_2}{\partial x^3}; \\
 x = l_1 : w_2 = w_3, \quad \frac{\partial w_2}{\partial x} = \frac{\partial w_3}{\partial x}, \\
 (EI)' \frac{\partial^2 w_2}{\partial x^2} - M_e = (EI)' \frac{\partial^2 w_3}{\partial x^2}, \quad (EI)' \frac{\partial^3 w_2}{\partial x^3} = (EI)' \frac{\partial^3 w_3}{\partial x^3}; \\
 x = l_2 : w_3 = w_4, \quad \frac{\partial w_3}{\partial x} = \frac{\partial w_4}{\partial x}, \\
 (EI)' \frac{\partial^2 w_3}{\partial x^2} = (EI)' \frac{\partial^2 w_4}{\partial x^2} - M_e, \quad (EI)' \frac{\partial^3 w_3}{\partial x^3} = (EI)' \frac{\partial^3 w_4}{\partial x^3}; \\
 x = L : \frac{\partial^2 w_4}{\partial x^2} = 0, \quad \frac{\partial^3 w_4}{\partial x^3} = 0.
 \end{aligned} \tag{B-3}$$

Appendix C Boundary and continuity conditions of beams under scan vibration tuning for delamination identification

I. Boundary and continuity conditions of delaminated beams if $L_2 < L_{d1}$ as shown in Fig. C-

1:

$$\begin{aligned}
 x = 0 : w_1 = 0, \quad \frac{\partial w_1}{\partial x} = 0 ; \\
 x = L_1 : w_1 = w_2, \quad \frac{\partial w_1}{\partial x} = \frac{\partial w_2}{\partial x}, \\
 (EI)' \frac{\partial^2 w_1}{\partial x^2} - M_e = (EI)' \frac{\partial^2 w_2}{\partial x^2}, \quad (EI)' \frac{\partial^3 w_1}{\partial x^3} = (EI)' \frac{\partial^3 w_2}{\partial x^3}; \\
 x = L_2 : w_2 = w_3, \quad \frac{\partial w_2}{\partial x} = \frac{\partial w_3}{\partial x}, \\
 (EI)' \frac{\partial^2 w_2}{\partial x^2} = (EI)' \frac{\partial^2 w_3}{\partial x^2} - M_e, \quad (EI)' \frac{\partial^3 w_2}{\partial x^3} = (EI)' \frac{\partial^3 w_3}{\partial x^3}; \\
 x = L_{d1} : w_3 = w_4, \quad \frac{\partial w_3}{\partial x} = \frac{\partial w_4}{\partial x}, \quad w_3 = w_5, \quad \frac{\partial w_3}{\partial x} = \frac{\partial w_5}{\partial x}, \\
 (EI)' \frac{\partial^2 w_3}{\partial x^2} = (EI)' \frac{\partial^2 w_4}{\partial x^2} + (EI)' \frac{\partial^2 w_5}{\partial x^2}, \quad (EI)' \frac{\partial^3 w_3}{\partial x^3} = (EI)' \frac{\partial^3 w_4}{\partial x^3} + (EI)' \frac{\partial^3 w_5}{\partial x^3}; \\
 x = L_{d2} : w_4 = w_6, \quad \frac{\partial w_4}{\partial x} = \frac{\partial w_6}{\partial x}, \quad w_5 = w_4, \quad \frac{\partial w_5}{\partial x} = \frac{\partial w_6}{\partial x}, \\
 (EI)' \frac{\partial^2 w_4}{\partial x^2} + (EI)' \frac{\partial^2 w_5}{\partial x^2} = (EI)' \frac{\partial^2 w_6}{\partial x^2}, \quad (EI)' \frac{\partial^3 w_4}{\partial x^3} + (EI)' \frac{\partial^3 w_5}{\partial x^3} = (EI)' \frac{\partial^3 w_6}{\partial x^3}; \\
 x = L : \frac{\partial^2 w_6}{\partial x^2} = 0, \quad \frac{\partial^3 w_6}{\partial x^3} = 0.
 \end{aligned} \tag{C-1}$$

II. Boundary and continuity conditions of delaminated beams if $L_1 < L_{d1}$ and $L_2 > L_{d1}$ as shown in Fig. C-2:

$$\begin{aligned}
x = 0 : w_1 = 0, \quad \frac{\partial w_1}{\partial x} = 0 ; \\
x = L_1 : w_1 = w_2, \quad \frac{\partial w_1}{\partial x} = \frac{\partial w_2}{\partial x}, \\
(EI)' \frac{\partial^2 w_1}{\partial x^2} - M_e = (EI)' \frac{\partial^2 w_2}{\partial x^2}, \quad (EI)' \frac{\partial^3 w_1}{\partial x^3} = (EI)' \frac{\partial^3 w_2}{\partial x^3}; \\
x = L_{d1} : w_2 = w_3, \quad \frac{\partial w_2}{\partial x} = \frac{\partial w_3}{\partial x}, \quad w_2 = w_4, \quad \frac{\partial w_2}{\partial x} = \frac{\partial w_4}{\partial x}, \\
(EI)' \frac{\partial^2 w_2}{\partial x^2} = (EI)' \frac{\partial^2 w_3}{\partial x^2} + (EI)' \frac{\partial^2 w_4}{\partial x^2}, \quad (EI)' \frac{\partial^3 w_2}{\partial x^3} = (EI)' \frac{\partial^3 w_3}{\partial x^3} + (EI)' \frac{\partial^3 w_4}{\partial x^3}; \\
x = L_2 : w_3 = w_4, \quad \frac{\partial w_3}{\partial x} = \frac{\partial w_4}{\partial x}, \quad w_3 = w_5, \quad \frac{\partial w_3}{\partial x} = \frac{\partial w_5}{\partial x}, \quad w_3 = w_6, \quad \frac{\partial w_3}{\partial x} = \frac{\partial w_6}{\partial x}, \\
(EI)' \frac{\partial^2 w_3}{\partial x^2} + (EI)' \frac{\partial^2 w_4}{\partial x^2} = (EI)' \frac{\partial^2 w_5}{\partial x^2} + (EI)' \frac{\partial^2 w_6}{\partial x^2} - M_e, \\
(EI)' \frac{\partial^3 w_3}{\partial x^3} + (EI)' \frac{\partial^3 w_4}{\partial x^3} = (EI)' \frac{\partial^3 w_5}{\partial x^3} + (EI)' \frac{\partial^3 w_6}{\partial x^3}; \\
x = L_{d2} : w_5 = w_6, \quad \frac{\partial w_5}{\partial x} = \frac{\partial w_6}{\partial x}, \quad w_5 = w_7, \quad \frac{\partial w_5}{\partial x} = \frac{\partial w_7}{\partial x}, \\
(EI)' \frac{\partial^2 w_5}{\partial x^2} + (EI)' \frac{\partial^2 w_6}{\partial x^2} = (EI)' \frac{\partial^2 w_7}{\partial x^2}, \quad (EI)' \frac{\partial^3 w_5}{\partial x^3} + (EI)' \frac{\partial^3 w_6}{\partial x^3} = (EI)' \frac{\partial^3 w_7}{\partial x^3}; \\
x = L : \frac{\partial^2 w_7}{\partial x^2} = 0, \quad \frac{\partial^3 w_7}{\partial x^3} = 0.
\end{aligned} \tag{C-2}$$

III. Boundary and continuity conditions of delaminated beams if $L_1 > L_{d1}$ and $L_2 < L_{d2}$ as shown in Fig. C-3:

$$\begin{aligned}
x = 0 : w_1 = 0, \quad \frac{\partial w_1}{\partial x} = 0 ; \\
x = L_{d1} : w_1 = w_2, \quad \frac{\partial w_1}{\partial x} = \frac{\partial w_2}{\partial x}, w_1 = w_3, \quad \frac{\partial w_1}{\partial x} = \frac{\partial w_3}{\partial x}, \\
(EI)' \frac{\partial^2 w_1}{\partial x^2} = (EI)' \frac{\partial^2 w_2}{\partial x^2} + (EI)' \frac{\partial^2 w_3}{\partial x^2}, \quad (EI)' \frac{\partial^3 w_1}{\partial x^3} = (EI)' \frac{\partial^3 w_2}{\partial x^3} + (EI)' \frac{\partial^3 w_3}{\partial x^3}; \\
x = L_1 : w_2 = w_3, \quad \frac{\partial w_2}{\partial x} = \frac{\partial w_3}{\partial x}, w_2 = w_4, \quad \frac{\partial w_2}{\partial x} = \frac{\partial w_4}{\partial x}, \quad w_2 = w_5, \quad \frac{\partial w_2}{\partial x} = \frac{\partial w_5}{\partial x}, \\
(EI)' \frac{\partial^2 w_2}{\partial x^2} + (EI)' \frac{\partial^2 w_3}{\partial x^2} - M_e = (EI)' \frac{\partial^2 w_4}{\partial x^2} + (EI)' \frac{\partial^2 w_5}{\partial x^2}, \\
(EI)' \frac{\partial^3 w_2}{\partial x^3} + (EI)' \frac{\partial^3 w_3}{\partial x^3} = (EI)' \frac{\partial^3 w_4}{\partial x^3} + (EI)' \frac{\partial^3 w_5}{\partial x^3}; \\
x = L_2 : w_4 = w_5, \quad \frac{\partial w_4}{\partial x} = \frac{\partial w_5}{\partial x}, \quad w_4 = w_6, \quad \frac{\partial w_4}{\partial x} = \frac{\partial w_6}{\partial x}, \quad w_4 = w_7, \quad \frac{\partial w_4}{\partial x} = \frac{\partial w_7}{\partial x}, \\
(EI)' \frac{\partial^2 w_4}{\partial x^2} + (EI)' \frac{\partial^2 w_5}{\partial x^2} = (EI)' \frac{\partial^2 w_6}{\partial x^2} + (EI)' \frac{\partial^2 w_7}{\partial x^2} - M_e, \\
(EI)' \frac{\partial^3 w_4}{\partial x^3} + (EI)' \frac{\partial^3 w_5}{\partial x^3} = (EI)' \frac{\partial^3 w_6}{\partial x^3} + (EI)' \frac{\partial^3 w_7}{\partial x^3}; \\
x = L_{d2} : w_6 = w_7, \quad \frac{\partial w_6}{\partial x} = \frac{\partial w_7}{\partial x}, w_6 = w_8, \quad \frac{\partial w_6}{\partial x} = \frac{\partial w_8}{\partial x}, \\
(EI)' \frac{\partial^2 w_6}{\partial x^2} + (EI)' \frac{\partial^2 w_7}{\partial x^2} = (EI)' \frac{\partial^2 w_8}{\partial x^2}, (EI)' \frac{\partial^3 w_6}{\partial x^3} + (EI)' \frac{\partial^3 w_7}{\partial x^3} = (EI)' \frac{\partial^3 w_8}{\partial x^3}; \\
x = L : \frac{\partial^2 w_8}{\partial x^2} = 0, \quad \frac{\partial^3 w_8}{\partial x^3} = 0.
\end{aligned} \tag{C-3}$$

IV. Boundary and continuity conditions of delaminated beams if $L_1 < L_{d2}$ and $L_2 > L_{d2}$ as shown in Fig. C-4:

$$\begin{aligned}
x = 0 : w_1 = 0, \quad \frac{\partial w_1}{\partial x} = 0 ; \\
x = L_{d1} : w_1 = w_2, \quad \frac{\partial w_1}{\partial x} = \frac{\partial w_2}{\partial x}, \quad w_1 = w_3, \quad \frac{\partial w_1}{\partial x} = \frac{\partial w_3}{\partial x}, \\
(EI)' \frac{d^2 w_1}{dx^2} = (EI)' \frac{\partial^2 w_2}{\partial x^2} + (EI)' \frac{\partial^2 w_3}{\partial x^2}, \quad (EI)' \frac{\partial^3 w_1}{\partial x^3} = (EI)' \frac{\partial^3 w_2}{\partial x^3} + (EI)' \frac{\partial^3 w_3}{\partial x^3}; \\
x = L_1 : w_2 = w_3, \quad \frac{\partial w_2}{\partial x} = \frac{\partial w_3}{\partial x}, \quad w_2 = w_4, \quad \frac{\partial w_2}{\partial x} = \frac{\partial w_4}{\partial x}, w_2 = w_5, \quad \frac{\partial w_2}{\partial x} = \frac{\partial w_5}{\partial x}, \\
(EI)' \frac{\partial^2 w_2}{\partial x^2} + (EI)' \frac{\partial^2 w_3}{\partial x^2} - M_e = (EI)' \frac{\partial^2 w_4}{\partial x^2} + (EI)' \frac{\partial^2 w_5}{\partial x^2}, \\
(EI)' \frac{\partial^3 w_2}{\partial x^3} + (EI)' \frac{\partial^3 w_3}{\partial x^3} = (EI)' \frac{\partial^3 w_4}{\partial x^3} + (EI)' \frac{\partial^3 w_5}{\partial x^3}; \\
x = L_{d2} : w_4 = w_5, \quad \frac{\partial w_4}{\partial x} = \frac{\partial w_5}{\partial x}, \quad w_4 = w_6, \quad \frac{\partial w_4}{\partial x} = \frac{\partial w_6}{\partial x}, \\
(EI)' \frac{\partial^2 w_4}{\partial x^2} + (EI)' \frac{\partial^2 w_5}{\partial x^2} = (EI)' \frac{\partial^2 w_6}{\partial x^2}, \quad (EI)' \frac{\partial^3 w_4}{\partial x^3} + (EI)' \frac{\partial^3 w_5}{\partial x^3} = (EI)' \frac{\partial^3 w_6}{\partial x^3}; \\
x = L_2 : w_6 = w_7, \quad \frac{\partial w_6}{\partial x} = \frac{\partial w_7}{\partial x}, \\
(EI)' \frac{\partial^2 w_6}{\partial x^2} = (EI)' \frac{\partial^2 w_7}{\partial x^2} - M_e, (EI)' \frac{\partial^3 w_6}{\partial x^3} = (EI)' \frac{\partial^3 w_7}{\partial x^3}; \\
x = L : \frac{\partial^2 w_7}{\partial x^2} = 0, \quad \frac{\partial^3 w_7}{\partial x^3} = 0.
\end{aligned} \tag{C-4}$$

V. Boundary and continuity conditions of delaminated beams if $L_1 > L_{d2}$ as shown in Fig. C-5:

$$\begin{aligned}
x = 0 : w_1 = 0, \quad \frac{\partial w_1}{\partial x} = 0 ; \\
x = L_{d1} : w_1 = w_2, \quad \frac{\partial w_1}{\partial x} = \frac{\partial w_2}{\partial x}, w_1 = w_3, \quad \frac{\partial w_1}{\partial x} = \frac{\partial w_3}{\partial x}, \\
(EI)' \frac{\partial^2 w_1}{\partial x^2} = (EI)' \frac{\partial^2 w_2}{\partial x^2} + (EI)' \frac{\partial^2 w_3}{\partial x^2}, \quad (EI)' \frac{\partial^3 w_1}{\partial x^3} = (EI)' \frac{\partial^3 w_2}{\partial x^3} + (EI)' \frac{\partial^3 w_3}{\partial x^3}; \\
x = L_{d2} : w_2 = w_3, \quad \frac{\partial w_2}{\partial x} = \frac{\partial w_3}{\partial x}, w_2 = w_4, \quad \frac{\partial w_2}{\partial x} = \frac{\partial w_4}{\partial x}, \\
(EI)' \frac{\partial^2 w_2}{\partial x^2} + (EI)' \frac{\partial^2 w_3}{\partial x^2} = (EI)' \frac{\partial^2 w_4}{\partial x^2}, \quad (EI)' \frac{\partial^3 w_2}{\partial x^3} + (EI)' \frac{\partial^3 w_3}{\partial x^3} = (EI)' \frac{\partial^3 w_4}{\partial x^3}; \\
x = L_1 : w_4 = w_5, \quad \frac{\partial w_4}{\partial x} = \frac{\partial w_5}{\partial x}, \\
(EI)' \frac{\partial^2 w_4}{\partial x^2} - M_e = (EI)' \frac{\partial^2 w_5}{\partial x^2}, \quad (EI)' \frac{\partial^3 w_4}{\partial x^3} = (EI)' \frac{\partial^3 w_5}{\partial x^3}; \\
x = L_2 : w_5 = w_6, \quad \frac{\partial w_5}{\partial x} = \frac{\partial w_6}{\partial x}, \\
(EI)' \frac{\partial^2 w_5}{\partial x^2} = (EI)' \frac{\partial^2 w_6}{\partial x^2} - M_e, \quad (EI)' \frac{\partial^3 w_5}{\partial x^3} = (EI)' \frac{\partial^3 w_6}{\partial x^3}; \\
x = L : \frac{\partial^2 w_6}{\partial x^2} = 0, \quad \frac{\partial^3 w_6}{\partial x^3} = 0.
\end{aligned} \tag{C-5}$$

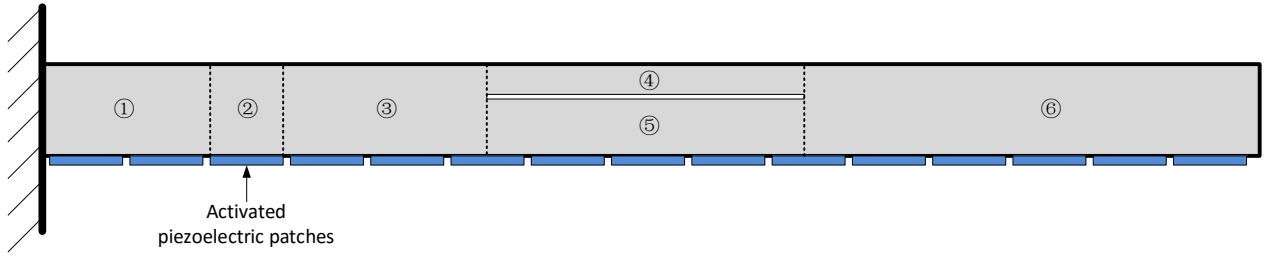


Fig. C-1 Physical model of a delaminated beam coupled with piezoelectric patches when $L_2 < L_{d1}$

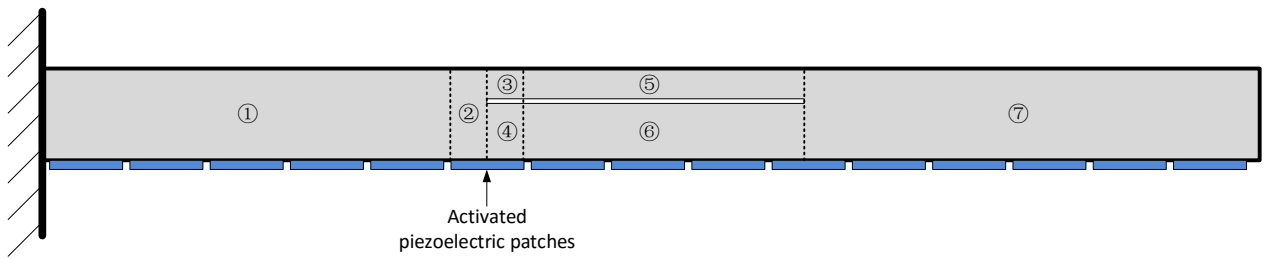


Fig. C-2 Physical model of a delaminated beam coupled with piezoelectric patches when $L_1 < L_{d1}$ and $L_2 > L_{d1}$

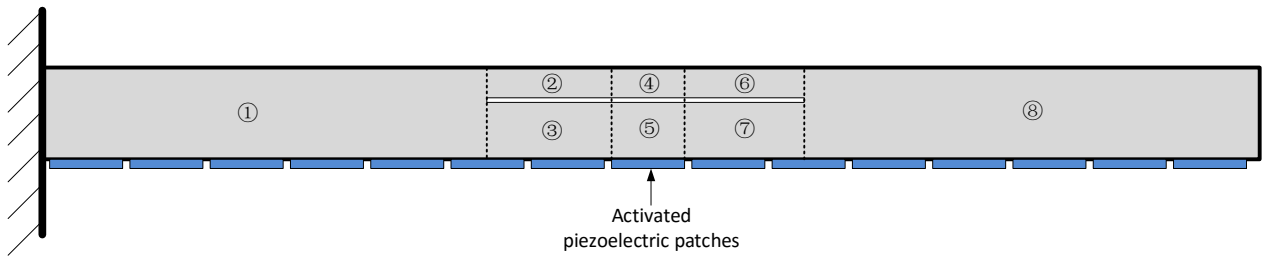


Fig. C-3 Physical model of a delaminated beam coupled with piezoelectric patches when $L_1 > L_{d1}$ and $L_2 < L_{d2}$

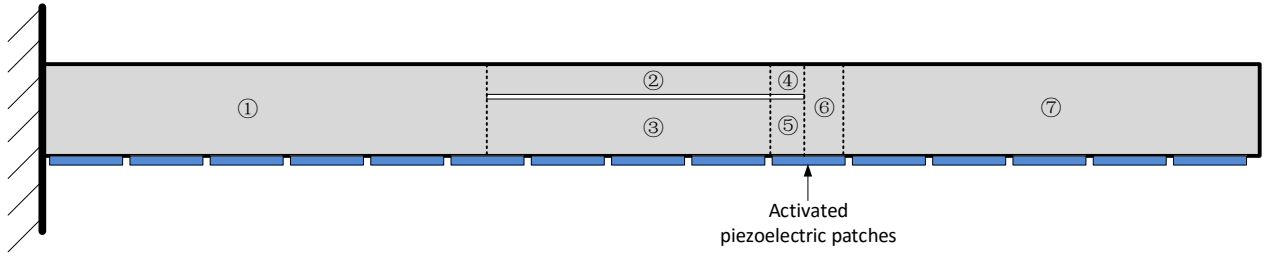


Fig. C-4 Physical model of a delaminated beam coupled with piezoelectric patches when $L_1 < L_{d2}$ and $L_2 > L_{d2}$

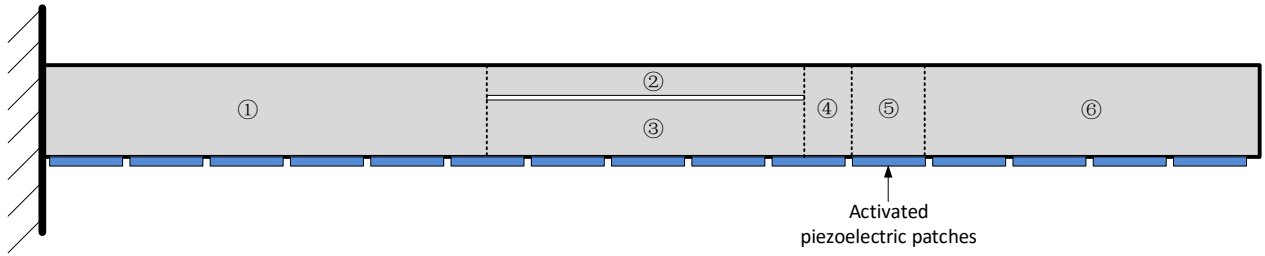


Fig. C-5 Physical model of a delaminated beam coupled with piezoelectric patches when $L_1 > L_{d2}$

Appendix D List of publications

Published (3):

- I. S. Zhao, N. Wu, Q. Wang, Damage Detection of Beams by a Vibration Characteristic Tuning Technique Through an Optimal Design of Piezoelectric Layers, International Journal of Structural Stability and Dynamics, (2015) 1550070.
- II. S. Zhao, N. Wu, Y. Cheng, High Sensitivity Damage Detection With Vibration Mode Shape Tuning Through the Optimal Design of Piezoelectric Actuators, in: ASME 2015 International Mechanical Engineering Congress and Exposition, American Society of Mechanical Engineers, 2015, pp. V04BT04A038-V004BT004A038.
- III. Y. Cheng, N. Wu, S. Zhao, Study on High Efficiency Energy Harvesting Using Piezoelectric Coupled Beam With Self-Tuning Process, in: ASME 2015 International Mechanical Engineering Congress and Exposition, American Society of Mechanical Engineers, 2015, pp. V04BT04A047-V004BT004A047.